Cerebral Cortex March 2011;21:666-682
doi:10.1093/cercor/bhq138
Advance Access publication August 12, 2010

Rapid Developmental Maturation of Neocortical FS Cell Intrinsic Excitability

Ethan M. Goldberg[1,2], Hyo-Young Jeong[3,4], Ilya Kruglikov[3,4], Robin Tremblay[3,4], Roman M. Lazarenko[5] and Bernardo Rudy[3,4,6]

[1]Department of Pediatrics, Division of Neurology, The Children's Hospital of Philadelphia, Abramson Research Center, Philadelphia, PA, 19104, [2]Department of Neurology, Hospital of the University of Pennsylvania, Philadelphia, PA, 19104, [3]Department of Physiology and Neuroscience and [4]Smilow Neuroscience Program, New York University School of Medicine, New York, NY 10016, USA, [5]Department of Pharmacology, University of Virginia, Charlottesville, VA 22908, USA and [6]Department of Biochemistry, New York University School of Medicine, New York, NY 10016, USA

Address correspondence to Bernardo Rudy. Email: bernardo.rudy@nyumc.org.

Fast-spiking (FS) cells are a prominent subtype of neocortical γ-aminobutyric acidergic interneurons that mediate feed-forward inhibition and the temporal sculpting of information transfer in neural circuits, maintain excitation/inhibition balance, and contribute to network oscillations. FS cell dysfunction may be involved in the pathogenesis of disorders such as epilepsy, autism, and schizophrenia. Mature FS cells exhibit coordinated molecular and cellular specializations that facilitate rapid responsiveness, including brief spikes and sustained high-frequency discharge. We show that these features appear during the second and third postnatal weeks driven by upregulation of K^+ channel subunits of the Kv3 subfamily. The low membrane resistance and fast time constant characteristic of FS cells also appears during this time, driven by expression of a K^+ leak current mediated by $K_{ir}2$ subfamily inward rectifier K^+ channels and TASK subfamily 2-pore K^+ channels. Blockade of this leak produces dramatic depolarization of FS cells suggesting the possibility for potent neuromodulation. Finally, the frequency of FS cell membrane potential oscillations increases during development and is markedly slower in TASK-1/3 knockout mice, suggesting that TASK channels regulate FS cell rhythmogenesis. Our findings imply that some of the effects of acidosis and/or anesthetics on brain function may be due to blockade of TASK channels in FS cells.

Keywords: FS cells, interneurons, neocortex, potassium channels

Introduction

Neocortical fast-spiking **(FS)** γ-aminobutyric acidergic (GABAergic) interneurons (FS cells) exhibit a constellation of features that are coordinated for rapid response and high temporal precision. FS cells discharge sustained nonaccomadating trains of brief action potentials (APs) at frequencies higher than any other cortical neuron, a feature that requires the specific expression of voltage-gated potassium channels (K^+ channels) of the Kv3 subfamily (reviewed in Rudy and McBain 2003). FS cells have also been shown to differentially express sodium (Na^+) channels that recover from inactivation rapidly (Martina and Jonas 1997). In addition, FS cells have a lower input resistance (R_m) and hence a fast membrane time constant (τ_m) relative to excitatory neocortical neurons as well as non-FS GABAergic interneurons (e.g., Kawaguchi 1995; Beierlein et al. 2003; Jonas et al. 2004; Goldberg and Rudy 2005). Furthermore, glutamatergic synaptic inputs onto FS cells produce excitatory postsynaptic currents with fast kinetics due to the expression of alpha-amino-3-hydroxyl-5-methyl-4-isoxazole-propionate (AMPA) receptors containing $GluR1_{flop}$ and lacking GluR2 (Geiger et al. 1995, 1997; Angulo et al. 1997; Hull et al. 2009). FS cell-mediated synaptic output is in turn characterized by rapid and synchronous neurotransmitter release, which is produced in part by tight coupling between calcium (Ca^{2+}) entry and neurotransmitter release machinery via P/Q-type voltage-gated Ca^{2+} channels (Hefft and Jonas 2005). FS cells also express synaptically localized Kv3 channels that keep spikes brief at the synaptic terminal and thereby limit spike-induced Ca^{2+} influx and short-term synaptic depression (Goldberg et al. 2005). The above features are thought to be important for the hypothesized roles of FS cells in a host of cortical operations, such as feed-forward inhibition, which is important for creating a strict window for temporal summation and spike generation by principal cells (Pouille and Scanziani 2001; Lawrence and McBain 2003; Gabernet et al. 2005; Cruikshank et al. 2007), the maintenance of excitation/inhibition balance, regulation of experience-dependent plasticity (e.g., Hensch 2005), and the establishment and maintenance of fast network oscillations (Traub et al. 2004; Bartos et al. 2007; Cardin et al. 2009).

However, it has been shown in multiple mammalian species that the GABAergic system develops slowly during early postnatal life, including with regard to the sign of the GABAergic response (i.e., whether GABAergic responses are depolarizing or hyperpolarizing), processes such as axonal arborization and the subcellular targeting and molecular organization of GABAergic synapses, short-term synaptic plasticity at GABAergic synapses, the establishment of network rhythmogenesis, as well as activity-dependent neuroplasticity (Ben-Ari 2002; Owens and Kriegstein 2002; Hensch 2005; Jiang et al. 2005; Huang et al. 2007). A "window" between the maturation of excitatory and inhibitory subsystems has been hypothesized to regulate experience-dependent plasticity in the neocortex such that a particular level of excitation/inhibition balance might be "permissive" for plasticity, and/or the development of inhibition may have a role in "closing" a critical period (Hensch 2005; Jiang et al. 2005; Gandhi et al. 2008). Finally, disruption or alteration in the maturation of inhibition has been hypothesized to play a role in the pathogenesis of various neurologic and psychiatric disorders, including schizophrenia, autism, and epilepsy (Levitt et al. 2004; Lewis et al. 2005; Walsh et al. 2008).

Data exist to suggest that, much like the GABAergic system overall, cortical FS cells in particular develop dramatically during early postnatal life. For example, the K^+ channel subunits Kv3.1 and Kv3.2, which determine the FS behavior characteristic of FS cells, are known to exhibit a developmentally regulated expression pattern among hippocampal

interneurons (Du et al. 1996; Tansey et al. 2002; Itami et al. 2007; Doischer et al. 2008; Okaty et al. 2009).

Here, we extend previous studies on the developmental maturation of FS interneurons by performing a fine-grained analysis of the postnatal changes that occur in FS cell intrinsic neurophysiological properties. Our work indicates that multiple features of the neocortical FS cell rapid-response phenotype appear during the second and third postnatal weeks. First, we show that the features that classically define the FS cell—including the presence of thin spikes (i.e., short action potential half-width [AP ½-width]), the discharge of sustained trains of APs at high frequency in response to sustained depolarization, and the ability to reliably follow repetitive high-frequency excitatory inputs—are absent in immature FS cells but appear during a remarkably brief postnatal time window driven by the developmentally regulated expression of K^+ channel subunits Kv3.1 and Kv3.2. Second, during this very same time interval, the FS cell resting membrane potential (RMP) becomes more hyperpolarized, input resistance falls, and membrane time constant decreases, all features also characteristic of mature FS cells. Our data suggest that the molecular basis of these changes in passive membrane properties is the developmental upregulation of the inward rectifier K^+ (K_{ir}) channel subunits $K_{ir}2.2$ and $K_{ir}2.3$ as well as 2-pore domain-containing K+ (K_{2P}) channel subunits of the TASK subfamily with a possible contribution of TWIK-1. We also show that these changes in FS cell passive membrane properties correlate with a shift from θ- to γ-band near-threshold membrane potential oscillations.

The developmental changes in FS cell discharge patterns, passive membrane properties, subthreshold behavior, and synaptic properties shown here may have important consequences for the hypothesized and known roles of FS cells in mature brain microcircuits as well as the theorized involvement of FS cells in various neurodevelopmental disorders.

These results have been presented previously in abstract form Goldberg and Rudy (2005).

Materials and Methods

Slice Preparation

All experiments were carried out in accordance with the NIH Guide for the Care and Use of Laboratory Animals. Acute brain slices were prepared from mice (10–60 days old) using standard techniques (Stuart and Sakmann 1995) essentially as previously described (Goldberg et al. 2008).

Cell Selection

Cells were visualized using a ×40, 0.8 NA water-immersion objective (Olympus) on an Olympus BX-50 upright microscope equipped with infrared differential interference contrast optics. FS cells can generally be distinguished from pyramidal cells (PCs) in layer 2/3 mouse barrel cortex using established criteria (Goldberg et al. 2005, 2008). We also used bacterial artificial chromosome transgenic mice in which expression of green fluorescent protein (GFP) is present in neurons that express the calcium-binding protein parvalbumin (PV) (PV being a known marker of FS cells; Kawaguchi and Kondo 2002), provided by Z. Josh Huang at Cold Spring Harbor Laboratories (Chattopadhyaya et al. 2004). These mice are further described in Goldberg et al. (2005, 2008).

Immunohistochemistry

Cells were routinely filled with bioctyin (0.5%) and processed "post hoc" using standard immunoperoxidase or immunofluorescence methods (Hamam and Kennedy 2003). Primary antibodies were: rabbit anti-somatostatin (Peninsula Labs; T-4103) and mouse anti-PV (Sigma; P-3088). Secondary antibodies were: Alexa 488-conjugated streptavidin (Molecular Probes; S-32354), Alexa 594 goat anti-rabbit (A-11022), and Alexa 350 goat anti-mouse (A-21049).

Electrophysiology

Whole-cell current and voltage clamp recordings were performed as previously described (Goldberg et al. 2005, 2008).

Apparent membrane resistance (R_m) in current clamp was calculated from the slope of the *V-I* curve, in the linear region of this curve, as constructed using small current injections around RMP. The *V-I* curve of FS cells was always near-linear near rest, although PCs often exhibited some deviation from linearity (see, e.g., Fig. 2*b*).

Membrane time constant (τ_m) was calculated using a single exponential fit of the voltage deflection produced by small hyperpolarizing current pulses from RMP.

AP ½-width was calculated as the width (in ms) of the AP at half-maximal height (defined as the amplitude from AP voltage threshold to AP peak).

The amplitude of the subthreshold membrane potential oscillations was quantified as the mean peak-to-trough amplitude of the oscillation period just prior to spiking at threshold.

Voltage ramps were performed by stepping the voltage from a holding potential of –70 mV instantly to –125 mV and then ramping the voltage from –125 to –45 mV in 4 s (at a slope of 20 mV/s). The reverse protocol (i.e., ramping from –45 to –125 mV) produced identical results (data not shown). Voltage ramp experiments were generally performed in the presence of 500 nM TTX (to block fast voltage-gated Na+ channels), 10 μM CNQX/50 μM D-APV (Tocris; to block spontaneous excitatory synaptic transmission), 10 μM SR-95531 (Tocris; to block spontaneous inhibitory synaptic transmission), and 10 μM ZD-7288 (Tocris; to block I_h). We did not observe any current sensitive to 0.5–1.0 μM TTX (Alomone Labs) in the voltage range of –125 to –45 mV. The inwardly rectifying appearance of the modified *I-V* plot at P18 or its block by Ba^{2+} persisted in the presence or absence of ZD-7288, 50 μM $CdCl_2$, and 50 μM $NiCl_2$; hence, the effect of Ba^{2+} is not due to block of I_h or to Ba^{2+} flux through voltage-gated calcium channels.

Perforated Patch Recordings

For perforated patch recordings, gramicidin-D (Sigma; G-5002) was prepared as a stock solution in DMSO (10 mg/mL) prior to the experiment and then diluted in pipette-filling solution to a final concentration of 20 μg/mL. Pipettes were front filled with gramicidin-free internal solution and back filled with internal solution containing gramicidin-D. Internal solution contained Alexa 594 (Molecular Probes; A-30677) as a control for rupture of the patch.

FACS Purification of FS Cells

Mice (10–18 days old) were deeply anesthetized and decapitated, and brains (up to 4 per experiment) were rapidly removed to continuously oxygenated, ice-cold artificial cerebrospinal fluid (ACSF) that contained in mM: NaCl 87; sucrose 75; KCl 2.5; NaH_2PO_4 1.25; $NaHCO_3$ 26; glucose 10; $CaCl_2$ 1; $MgSO_4$ 2; D-AP5 0.025; CNQX 0.01; and TTX 0.0001. Slices (400-μm thick) were cut on a vibratome and transferred to an incubation chamber containing the above solution, first for 15 min at 32 °C and then at room temperature for 15 min. Sensorimotor neocortex was then grossly dissected out using a scalpel, and tissue pieces were transferred to ACSF containing 2 mg/mL of pronase E (Sigma, P-5147) and 0.05 mg/mL of DNase (Worthington Biochem, LK003170) for 45 min. Pronase-treated tissue was washed with ACSF 3 times and transferred to 4-(2-hydroxyethyl)-1-piperazineethanesulfonic acid (HEPES)-based ACSF (in mM: NaCl, 150; HEPES, 10; KCl, 2.5; NaH_2PO_4, 1.25; glucose, 10; $CaCl_2$, 1.0; $MgSO_4$, 2.0; D-AP5, 0.025; CNQX, 0.01; TTX, 0.0001), pH 7.4 and bubbled with 100% O_2, and containing 1 mg/mL of albumin inhibitor (Worthington Biochem, LK003182) and 0.05 mg/mL of DNase. Tissue pieces were triturated with a series of Pasteur pipettes of decreasing size (fashioned to approximately 500-, 300-, and 200-μm tip opening) and filtered through a 70-μm mesh (BD Falcon; catalog number 352350).

Florescence-activated cell sorting (FACS) was performed at the NYU Cancer Institute's Flow Cytometry and Cell Sorting Facility with a DakoCytomation MoFlo equipped with a 5 W Argon Laser (488 nm) and 5 W Krypton laser (350 nm, 414 nm, and 568 nm). The instrument can measure 10 parameters simultaneously (forward- and right-angle scatter plus 8 fluorescence wavelengths). A primary gate based on physical parameters (forward and side light scatter; FSC and SSC, respectively) was set to exclude dead cells or debris. A 2-color flow cytometry experiment was performed with fluorescein for GFP positive cells and phycoerythrin for auto fluorescence. Sorting was generally performed at a rate of 1000 cells/s. GFP positive cells were sorted directly into a 96 well plate (for reverse transcriptase-polymerase chain reaction [RT-PCR]) or a tube (for real-time PCR) filled with TRIzol (Invitrogen; 15596-026) for subsequent analysis.

RNA Preparation and cDNA Synthesis

FACS-sorted cells in TRIzol reagent were transferred to 1.5 mL microcentrifuge tubes. Samples were incubated for 5 min at room temperature to permit complete dissociation of nucleoprotein complexes. Two hundred microliters of chloroform was added per 1 mL TRIzol reagent, and the tube was then shaken vigorously by hand for 15 s, followed by incubation at room temperature for 3 min. The samples were then centrifuged at 12 000 × *g* for 15 min at 4 °C. The aqueous phase was transferred to a fresh tube, and 500 μL of isopropyl alcohol was added. Samples were then incubated at –20 °C overnight, followed by centrifugation at 12 000 × *g* for 15 min at 4 °C. The supernatant was then removed, and the RNA pellet was washed once with 400 μL of 75% ethanol. The RNA pellet was then dried and dissolved in RNAase-free water. Reverse transcription was performed using the SuperScript III First-Strand Synthesis System for RT-PCR (Invitrogen; 18080-051), essentially as per the manufacturer's instructions, to produce first-strand cDNA, which was then used as a template for RT-PCR and real-time PCR.

Real-Time PCR

The ABI Prism 7900HT Sequence Detection System (Perkin-Elmer Applied Biosystems) was used to perform the real-time experiments using a 10-μL volume reaction in a 384 well plate. One microliter of RT reaction product and 5 picomoles of premixed primer pairs were mixed with Power SYBR Green PCR Master Mix in each well. The thermal cycling conditions were as follows: stage 1, at 50 °C for 2 min; stage 2, at 95 °C for 10 min; stage 3, 40 cycles at 95 °C for 15 s, and 60 °C for 1 min. Following this cycling condition, a melting curve analysis was performed by cooling the PCR product to 60 °C for 15 s before gradual heating (ramp rate of 1 °C/min) to 95 °C.

Western Blot and Immunohistochemistry

These experiments were performed using standard laboratory techniques (Weiser et al. 1995; Chow et al. 1999).

Results

Maturation of FS Cells Firing Properties

The firing pattern of FS neocortical GABAergic interneurons (FS cells) in rodent brain slice preparations is well characterized (Connors and Gutnick 1990; Kawaguchi 1995). Typical examples of an FS cell (Fig. 1*a*) and a PC (Fig. 1*c*) recorded from layer 2/3 barrel cortex of a postnatal day 18 (P18) mouse using whole-cell current clamp recordings in the acute brain slice preparation are shown in Figure 1. At P18 and later (P18+; up to and including P60) FS cells and PCs fall into 2 distinct and nonoverlapping clusters based upon AP ½-width (Fig. 2*a*) and apparent input resistance (R_m Fig. 2*a–b*). We also analyzed AP ½-width of spikes produced by brief depolarizing current

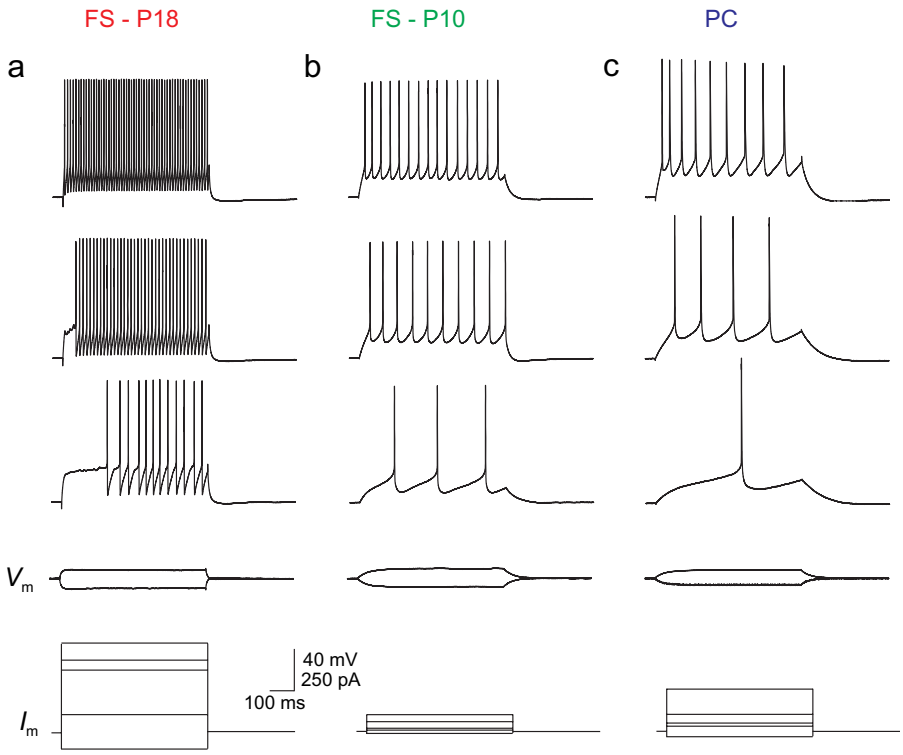

Figure 1. FS cells at P10 exhibit low firing frequency. (*a*) Discharge pattern of an FS cell in layer 2/3 barrel cortex at P18. Shown are voltage responses to 600-ms current injections of, from bottom to top, −100, 100, 360 (current threshold; ITH), 420, and 520 pA. Note the sustained discharge of nonaccommodating trains of brief APs at high frequency in response to depolarizing current injection, characteristic of FS cells. Scale bars in *a* apply to *b* and *c*. (*b*) As in 1*a*, for an FS cell in layer 2/3 barrel cortex from a mouse age P10. Shown are current steps of −10, 10, 20 (I_{TH}), 60, and 100 pA. Note the higher R_m, lower I_{TH}, and lower maximal firing frequency as compared with the FS cell at P18 shown in 1*a*. (*c*) Firing pattern of a typical PC in layer 2/3 barrel cortex from a P18 mouse. Current steps are −30, 30, 50 (I_{TH}), 100, and 250 pA.

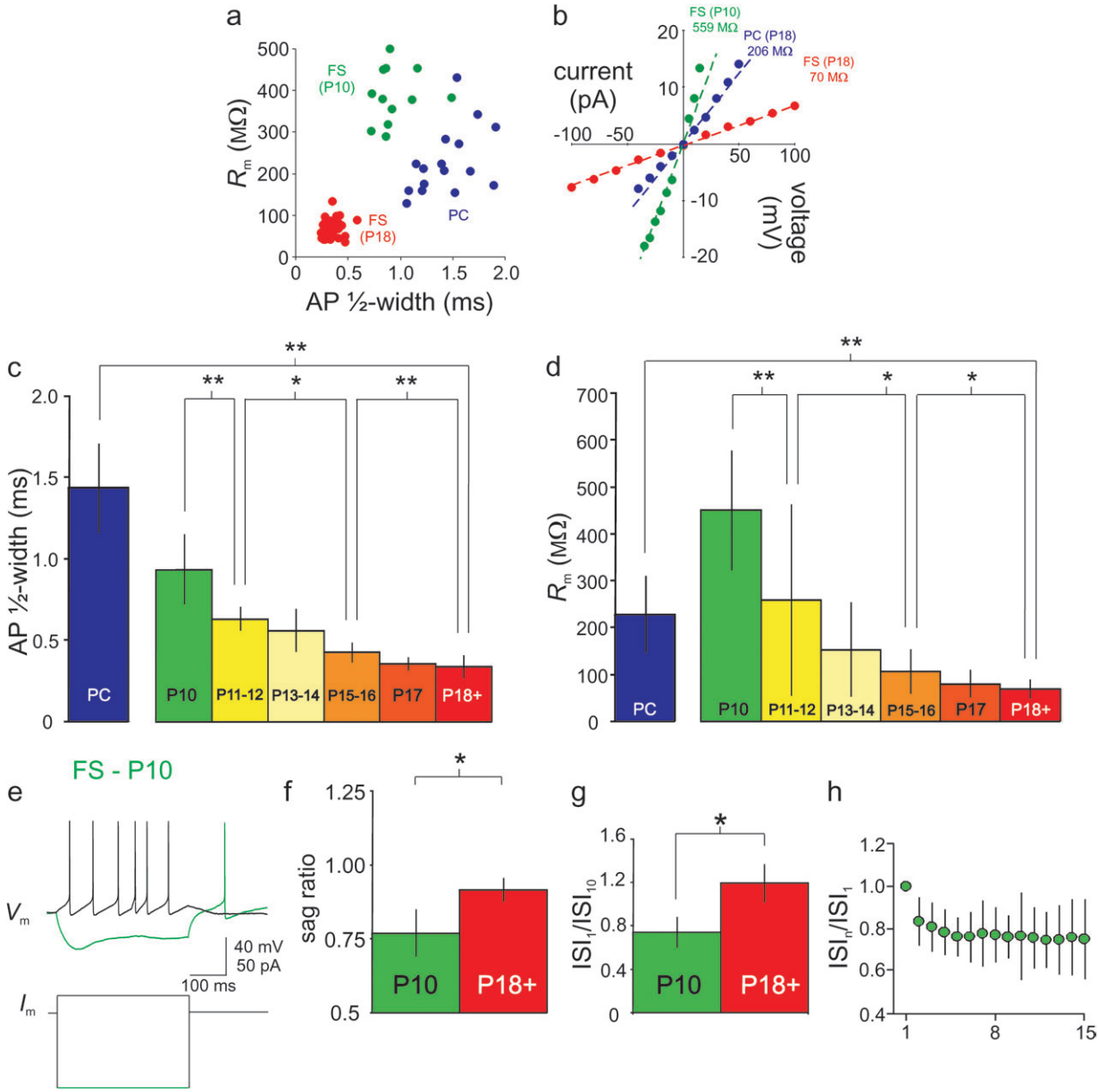

Figure 2. The brief spikes and low membrane time constant typical of mature FS cells develop during the second and third postnatal weeks. (*a*) Plot of input resistance (R_m; see Materials and Methods) versus AP ½-width (see Materials and Methods). FS cells at P18+ are indicated by red dots, FS cells at P10 by green dots, and PCs by blue dots. All cells resided in layer 2/3 barrel cortex. Note that FS cells at P18+ can be reliably and unequivocally distinguished from FS cells at P10 and from PCs by these 2 criteria and that the 3 populations are largely nonoverlapping with one another. (*b*) R_m was calculated as the linear fit to the voltage-current (*V-I*) plot constructed using small hyperpolarizing and depolarizing current injections near RMP. (*c*) Bar graph showing summary data for AP ½-width calculated for FS cells at various ages (P10, P11–12, P13–14, P15–16, P17, and P18+) and for PCs (P18+) (see Table 1). Asterisks indicate that interage differences reached statistical significance via Student's *t*-test (*$P < 0.05$; **$P < 0.01$) for this and all subsequent figures. Note the graded decrease in FS cell AP ½-width with age. (*d*) As in Figure 2*c*, for R_m. (*e*) Example of a P10 FS cell from layer 2/3 barrel cortex that exhibited prominent voltage sag and rebound spike on anode break. Sag ratio for this cell was 0.69. Consistent with the presence of a prominent voltage sag at P10, we were able to record a ZD-7288-sensitive current from these cells (not shown) confirming the presence of I_h. (*f*) Summary data illustrating greater voltage sag at P10 ($n = 9$) than at P18+ ($n = 46$). (*g*) Bar plot comparing the degree of spike frequency adaptation, as quantified by the ratio of the first to the tenth ISI (ISI_1/ISI_{10}), for FS cells at P10 versus P18+. (*h*) Summary data showing mean interspike intervals for each interval in the train (ISI_n) normalized to the first ISI in the train (ISI_1) for FS cells at P10 ($n = 11$). Note the appearance of moderate spike frequency adaptation.

injections and obtained near-identical results (data not shown). FS cells had brief single APs and a relatively low R_m compared with PCs (Figs 1 and 2) and to various types of non-FS interneurons (e.g., Supplementary Fig. S1), consistent with previous results (Kawaguchi 1995; Beierlein et al. 2003).

We then performed whole-cell recordings of FS cells at earlier postnatal ages (P10–P17). This was facilitated by the use of transgenic mice in which expression of enhanced green fluorescent protein (EGFP) is driven by the PV promoter (Chattopadhyaya et al. 2004), which enabled efficient targeting of FS cells for recording (PV being a specific marker for neocortical FS cells; Kawaguchi and Kondo 2002). In fact, this proved to be necessary, as FS cells exhibited strikingly different electrophysiological properties at progressively younger ages (see Materials and Methods). By recording from many cells at each postnatal day from P10 to P18 as well as P18+, the age

dependence of multiple electrophysiological parameters was observed to change in a graded fashion. It is unlikely that this would be the case were the GFP positive cells recorded in transgenic mice at young ages representative of a random or transient population. A subset of cells at P10 was filled with biocytin, and single-cell anatomy was visualized via post hoc immunohistochemistry. While putative FS cells at P10 were observed to have more simple dendritic arborizations and axonal extent, these cells were confirmed to be aspiny, multipolar cells (Supplementary Fig. S2), as are FS cells at P18+ (Kawaguchi 1995).

We first examined the discharge patterns of FS cells in layer 2/3 primary somatosensory cortex at various ages in response to depolarizing current injection. In contrast to FS cells at P18+ (Fig. 1*a*), FS cells at P10 fired trains of APs at low frequency (Fig. 1*b*), with moderate spike frequency adaptation (Fig. 2*g,b*). At P10, FS cell AP ½-width was 0.93 ± 0.21 ms (mean ± SD; $n = 17$), decreasing in a graded fashion to 0.34 ± 0.07 ($n = 48$) at P18+ (Fig. 2*a,c*; Table 1). We found that the developmental trajectory in spike width stabilized during the latter part of the third postnatal week. While there was a statistically significant difference in AP ½-width between P15–16 and P17 ($P < 0.01$ vs. P15–16), there was no difference between P17 and P18+ ($P > 0.05$ vs. P17) or between P18–29 and P30+ (0.31 ± 0.09 ms; $n = 5$; $P > 0.05$ vs. P18–29). Thus, in approximately 1 postnatal week (from P10 to P18), FS cell AP ½-width decreased dramatically (by >60%) and then stabilized at a mature value (at least up to P60, which was the latest time point assessed). That various indices of the FS phenotype (firing frequency, AP ½-width) are not present at P10 but emerge by P18 suggested that FS cells were immature at P10 but developed rapidly in the second and third postnatal weeks.

A relative lack of spike frequency adaptation during repetitive firing is a characteristic feature of FS cells (Connors and Gutnick 1990). We found that FS cells in layer 2/3 barrel cortex at P18+ lacked spike frequency adaptation, often exhibiting slight spike frequency acceleration (Goldberg et al. 2008): the ratio of the first interspike interval to the tenth interspike interval (ISI_1/ISI_{10}) during sustained trains of APs at high frequency was 1.19 ± 0.18 (mean ± SD; $n = 33$), while the ratio of ISI_1 to the last interspike interval (ISI_1/ISI_n) was 1.07 ± 0.24 (mean ± SD; $n = 32$). However, at P10, the ISI_1/ISI_n ratio (evoked at current injections that were twice the threshold current injection) was 0.74 ± 0.11 (mean ± SD; $n = 11$; $P < 0.01$ vs. P18+). This moderate spike frequency adaptation was present in P10 FS cells across current injections of all amplitudes, further consistent with an overall electrophysiological immaturity of FS cells at P10.

Another feature of mature FS cells is the lack of "voltage sag" along with an absence of rebound spiking upon anode break, the latter being a feature associated with a subset of somatostatin positive (SOM+), low-threshold spiking (LTS) interneurons known anatomically to be Martinotti cells (Kawaguchi and Kubota 1996, 2002; Goldberg et al. 2004). We quantified voltage sag as the ratio of peak to steady-state hyperpolarization in response to negative current injections (sag ratio): at P10, sag ratio was 0.77 ± 0.08 ($n = 9$); at P18+, sag was 0.92 ± 0.04 (mean ± SD; $n = 40$; $P < 0.05$) (Fig. 2*f*). Sag ratio among FS cells at P10 was similar to other cell types considered to have a prominent voltage sag, such as PCs of the subiculum and CA1 hippocampal subfield (0.79; Staff et al. 2000) and SOM+ neocortical LTS interneurons (0.77; Ma et al. 2006). Interestingly, of 17 FS cells recorded at P10, 2 exhibited rebound spiking (an example of which is shown in Fig. 2*e*). A rebound spike was never observed at P11+ ($n = 202$). This result demonstrates features of immature FS cells (sag; rebound spiking) observed at P10 that subsequently disappear.

We also found differences between P10 and P18+ in the amplitude and kinetics of the FS cell after-hyperpolarization, which are summarized in Table 1.

FS cells are further characterized by the ability to respond to repetitive high-frequency (>100 Hz) input in a reliable manner (Atzori et al. 2000). Further consistent with the emergence of the FS phenotype during the third postnatal week, we found that neocortical FS cells at P10 were unable to follow high-frequency stimulation (Fig. 3). The cutoff frequency (f_C; defined as the frequency beyond which the cell no longer responded in a 1:1 fashion relative to repetitive input) was, on

Table 1
Electrophysiological maturation of FS cells

Age	n	V_m (mV)[a]	R_m (MΩ)[b]	τ_m (ms)[c]	1/2-width (ms)[d]	AHP amp (mV)[e]	$t_{AHP,peak}$ (ms)[f]	$t_{AHP,90}$ (ms)[g]	$t_{AHP,peak-90}$ (ms)	ISI_1/ISI_{10}	ISI_1/ISI_n	max SFF (Hz)[h]	max IFF (Hz)[i]	sag (peak/ss)[j]
P10	17	−65.1 ± 4.3	448 ± 196	34.4 ± 6.8	0.93 ± 0.21	15.6 ± 4.0	18.6 ± 8.7	11.4 ± 5.6	7.1 ± 4.2	0.69 ± 0.09	0.73 ± 0.12	55 ± 26	75 ± 37	0.77 ± 0.08
P11–12	13	−67.8 ± 3.2	259 ± 202		0.63 ± 0.07	14.9 ± 3.7					0.78 ± 0.17	112 ± 43	147 ± 56	
P13–14	6	−68.6 ± 3.0	153 ± 99		0.56 ± 0.13	18.0 ± 3.2					0.97 ± 0.33	140 ± 79	175 ± 87	
P15–16	25	−69.4 ± 4.5	107 ± 47		0.43 ± 0.06	20.2 ± 8.9					0.93 ± 0.08	205 ± 75	241 ± 75	
P17	12	−73.7 ± 3.7	80 ± 29		0.36 ± 0.04	21.8 ± 2.8						>250	>250	
P18+	47	−71.5 ± 3.1	69 ± 19	5.7 ± 1.1	0.34 ± 0.07	18.7 ± 4.3	2.6 ± 1.5	2.0 ± 1.3	0.7 ± 0.6	1.19 ± 0.18	1.07 ± 0.24	>250	>250	0.92 ± 0.04

[a]RMP (V_m) was calculated by averaging membrane potential over one or more epochs of gap-free recording in which membrane potential was stable, and there were no spontaneous synaptic events (although many recordings were performed in the presence of pharmacological antagonists of synaptic transmission; see Materials and Methods).
[b]Input resistance (R_m) reported is resistance at/near rest as determined using the slope of the *V-I* curve (in the linear region of this curve) constructed using small hyperpolarizing and depolarizing pulses from rest.
[c]Membrane time constant (τ_m) was calculated using a single exponential fit of the voltage deflection produced by small hyperpolarizing current pulses from RMP (see Materials and Methods). This value was only calculated for P10 and P18+ data sets.
[d]AP ½-width was calculated as the width (in ms) of the AP at half-maximal height (defined as the amplitude from AP voltage threshold to AP peak).
[e]After-hyperpolarization amplitude (AHP amp) was defined as the voltage difference between voltage threshold and the depth of the AHP.
[f]Time to AHP peak ($t_{AHP,peak}$) reflects the time from AP threshold to depth of the AHP.
[g]Time to 90% of the AHP depth ($t_{AHP,90}$) refers to the time from AP threshold to the point at which the AHP had reached 90% maximal depth.
[h]Maximal steady-state firing frequency (max SFF) was defined as the maximal mean firing frequency achieved during 600-ms depolarizing current injections prior to AP failure (i.e., AP peak amplitude <0 mV). This value was not calculated for P17 and P18+ time points, although it was, on average, greater than 250 Hz.
[i]Maximal instantaneous firing frequency (max IFF) was defined as the inverse of the smallest observable ISI.
[j]See text.

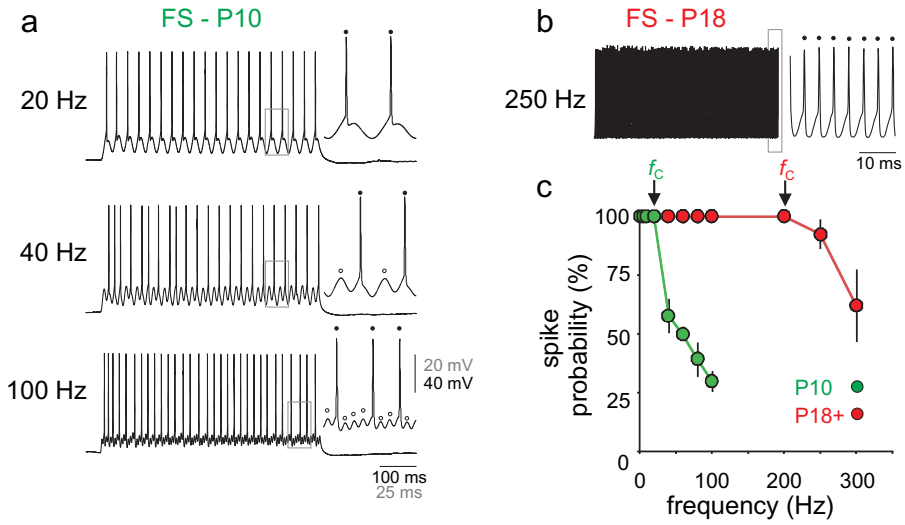

Figure 3. FS cells at P10 fail to reliably follow high-frequency input. (*a*) Response of an FS cell in layer 2/3 barrel cortex of a P10 mouse to sinusoidal current injection. The cell depicted in this example followed in a 1:1 fashion (1 AP per cycle) at frequencies up to 20 Hz ("top"), responded to approximately half (21/40) of cycles presented for 1 s at 40 Hz ("middle"), and to approximately one third (31/100) of cycles presented at 100 Hz ("bottom"). Insets at top, middle, and bottom show APs (indicated by "filled circles") and failures ("open circles") at greater detail (4-times magnification for areas demarcated by the "gray boxes"). (*b*) Response of a P18 FS cell to sinusoidal current injection. The cell depicted in this example successfully follows a sinusoidal current injection of 250 Hz in a 1:1 fashion (inset, 10-times horizontal magnification). (*c*) Summary data. Plotted is spike probability (percentage of cycles that generated an AP) versus frequency for FS cells at P10 ("green") and P18+ ("red"). The cutoff frequency, f_C, indicates the frequency beyond which cells no longer responded in a 1:1 fashion; note that f_C is approximately 10-fold greater at P18+ than at P10.

average, 26.7 ± 11.6 Hz (n = 3), and no FS cells at P10 were able to follow inputs at frequencies greater than approximately 40 Hz. In contrast, all FS cells tested at P18+ were able to reliably follow repetitive input at >200 Hz (n = 3; Fig. 3*b*,*c*).

We focused on FS cells in layer 2/3 in the present study, as neocortical FS cells are known to display subtle layer-specific differences in firing properties (Goldberg et al. 2008). However, we confirmed that FS cells in all layers (2–6) of barrel cortex exhibited the same basic phenomena shown here, with the appearance of high-frequency discharge, decrease in ½-width of FS cell APs, and decrease in FS cell R_m all proceeding with a similar developmental trajectory as in layer 2/3 barrel cortex (data not shown). For example, in layer 4, FS cell R_m was 281.7 ± 124.5 MΩ at P10 (n = 4) and 63.4 ± 17.0 at P18+ (n = 9; P < 0.01 vs. P10). We observed a similar but somewhat delayed developmental profile in medial prefrontal cortex (Goldberg and Rudy 2005).

Maturation of FS Cell Firing Properties Correlates with Kv3 Channel Protein Expression

The above electrophysiological data indicates that multiple indices of the FS phenotype of mouse neocortical FS cells appear during the second and third postnatal weeks, which strongly suggests a parallel developmental trajectory of the Kv3.1 and Kv3.2 proteins known to largely determine the FS behavior of these cells (Rudy and McBain 2001). Immunoblots for Kv3.1 (Fig. 4a_1) and Kv3.2 (Fig. 4a_2) performed on neocortical tissue extracts show this to be the case. Subsequent Kv3 immunostaining in tissue from mouse primary somatosensory cortex at P10 shows occasional weakly immunoreactive cell bodies along with sparse labeling of neuropil (likely FS cell axons and synaptic terminals; Weiser et al. 1995), while immunolabeling at P14 and to a progressively greater extent at P18 shows strong labeling of FS cell somata, axons, and perisynaptic terminals (Fig. 4*b*). Furthermore, quantitative PCR (qPCR) performed on FS cells purified using FACS (see Materials and Methods) at P10 and P18 indicated markedly greater relative Kv3.1 and Kv3.2 mRNA expression at P18 (Fig. 7*d*).

Maturation of FS Cell Synaptic Properties

We also compared FS cell synaptic connectivity at P10 and P18+. FS cells are well known to form efficacious perisomatic synapses with local excitatory neurons in neocortex that exhibit high release probability, low failure rate, and short-term synaptic depression (e.g., Beierlein et al. 2003). The paired-pulse ratio (PPR; defined as the ratio of the second postsynaptic potential (PSP) [PSP_2] to the first [PSP_1]) at FS→PC connections in layer 2/3 barrel cortex at P18+ was 0.71 ± 0.19 (n = 10) at 20 Hz, similar to other reported values (Galarreta and Hestrin 1998; Angulo et al. 2003; Goldberg et al. 2005). However, we found that the PPR of FS→PC connections at P10 was 0.53 ± 0.07 (mean ± SD; n = 6; P < 0.05 vs. P18+) (Fig. 5*a*–*c*), reflecting "stronger" paired-pulse depression at this early time point. We found that the failure rate of FS cell-to-PC synaptic transmission at P10 was 0.031 ± 0.027 (mean ± SD; range: 0–0.051; n = 5), extremely low, and similar to that at P18+.

Our previous work indicated that application of tetraethylammonium (TEA) ion produced a dramatic (near 2-fold) increase in the amplitude of evoked unitary GABA-mediated synaptic potentials in FS cell/PC pairs at P18+ via blockade of Kv3 channels specifically localized to FS cell basket terminals (Goldberg et al. 2005). Furthermore, we showed that synaptically localized Kv3 channels limit spike-evoked Ca^{2+} influx and short-term synaptic depression at FS cell synapses (Goldberg et al. 2005); hence, a lower PPR at FS cell-to-PC synapses at P10 (Fig. 5*b*) is consistent with less synaptic Kv3 channels at this time point (see Discussion). Further consistent with the absence of Kv3 protein in P10 FS cells, we find that 1.0 mM TEA has a small effect on FS cell-to-PC synaptic transmission at this age: the amplitude of the unitary GABA-mediated

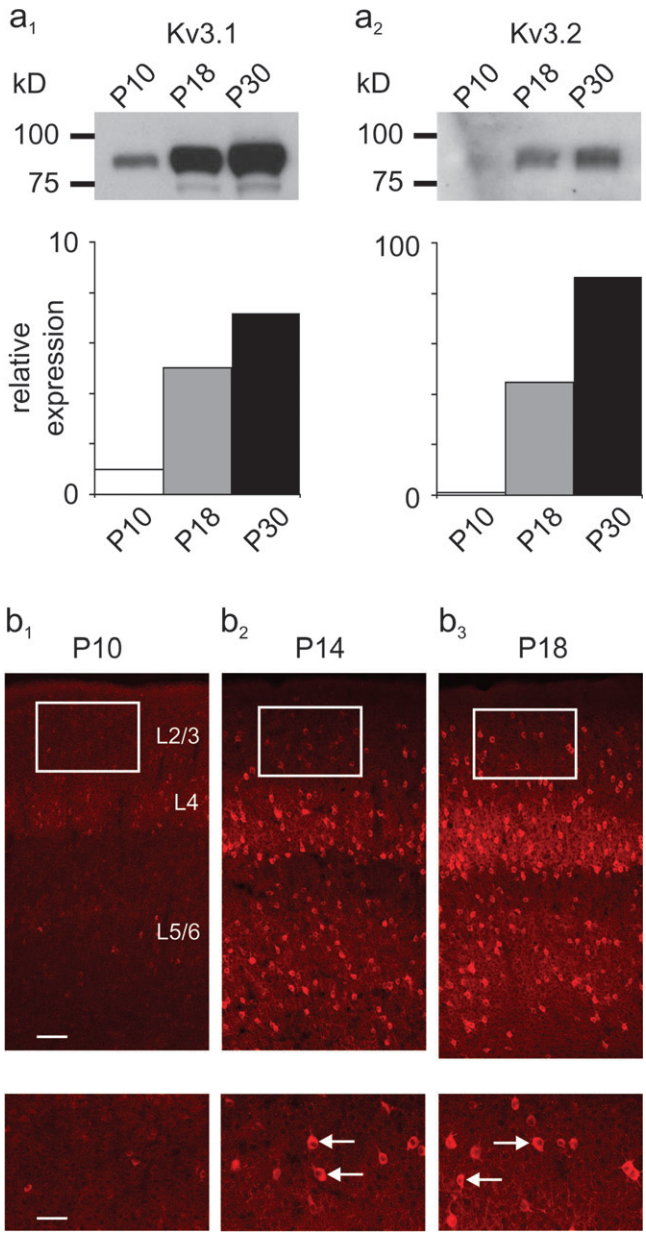

Figure 4. Kv3 proteins exhibit a developmentally regulated pattern of expression in mouse neocortex. (*a*) Immunoblots showing Kv3.1b (a_1) and Kv3.2 (a_2) protein expression in whole mouse neocortex at indicated ages (P10, 18, and 30). Note the weak Kv3.1 and near-absent Kv3.2 expression at P10, with dramatic upregulation by P18. Band intensities were quantified using ImageJ and normalized to P10 values: for Kv3.1, values increased to 5.03-times P10 levels at P18 and to 7.18-times P10 values at P30 (n = 2); for Kv3.2, values were 44.8-times P10 levels at P18 and 88.5-times P10 levels at P30 (n = 2). (*b*) Immunofluorescent histochemistry for Kv3.1b in mouse primary somatosensory cortex at P10 (b_1), P14 (b_2), and P18 (b_3). Boxed areas at "top" (×10 magnification) are shown at ×20 in the insets at "bottom." Note the occasional, weak staining of cell bodies with sparse labeling of neuropil at P10, compared with strong somatic staining and dense labeling of axons and perisomatic synapses at P18. Arrows in the insets in b_2 and b_3 indicate examples of labeled FS cell somata. Kv3.2 protein expression is qualitatively similar (Chow et al. 1999). Scale bars indicate 100 μM in b_1–b_3 and 50 μM in the insets.

postsynaptic current increased by 9 ± 4% after application of TEA (n = 3; P = 0.70), compared with a near 2-fold increase produced by TEA at P18+ (Goldberg et al. 2005, 2008).

In the course of these experiments, we observed that FS cells were interconnected by electrical synapses at P10 (Fig. 5*d*), although we did not examine this extensively (see Discussion). The coupling coefficient between electrically connected FS cells at P10 was 0.06 ± 0.02 (n = 4), which was similar to (although perhaps slightly smaller than) values previously reported for FS-FS electrical connections at 14–21 days of age in rat (Galarreta and Hestrin 1999; Gibson et al. 1999) and 2 months of age in mouse (Galarretta and Hestrin 2002).

Maturation of FS Cells Subthreshold Membrane Properties

Data presented thus far illustrate the dramatic changes in the nature of FS cell firing properties during development. FS cells also differ from PCs and non-FS interneurons in that FS cells possess a low input resistance, which in turn implies a fast membrane time constant (τ_m). At P18+, PC input resistance was 228.8 ± 80.1 MΩ (mean ± SD; n = 16), while FS cell input resistance was 69.1 ± 19.4 MΩ (mean ± SD; n = 49; P < 0.001 vs. PCs).

When we examined FS cells recorded from earlier postnatal time points, we found that R_m followed a similar developmental trajectory to that seen for AP ½-width and FS cell firing properties. Apparent R_m decreased from 484.5 ± 196.0 MΩ at P10 (mean ± SD; n = 17) to 69.1 ± 19.4 MΩ (n = 47) at ≥P18 (Fig. 2*a–b*; Table 1), a nearly 7-fold drop. As a result, FS cells at P10 have a larger (slower) τ_m, further illustrating the pervasive immaturity of the FS phenotype at this age: τ_m at P10 was 40.5 ± 9.8 ms (range: 32.5–59.0; n = 6) and decreased to 5.7 ± 1.1 ms at P18+ (range: 3.97–9.11 ms; n = 23; P < 0.01 vs. P10). This difference in τ_m was similar in magnitude to the difference in R_m between ages, suggesting that the surface area of the FS cell soma/proximal dendrite remained approximately the same (assuming a constant specific membrane capacitance between the 2 ages). Anatomical investigation did suggest that FS cells at P10 appear anatomically immature with regard to dendritic arborization (Supplementary Fig. S2), but the large surface area of distal dendritic and axonal branches is presumably not reflected to a great extent in estimates of capacitance measurements based on somatic current injections.

While the developmental trajectory of the FS cell firing properties parallels the decrease in R_m, the underlying mechanism of these 2 phenomena are likely to be different. The decrease in FS cell R_m cannot be caused by upregulation of Kv3 protein because the uniquely positive voltage dependence of activation of K^+ channels composed of Kv3 subunits ($V_{½}$ of activation of +15 mV; Rudy and McBain 2001) renders it such that Kv3 channels do not contribute significant current below –10 mV. In addition, we find that application of 1.0 mM TEA (which blocks Kv3 channels; Rudy et al. 2009) had no effect on apparent R_m calculated at rest at P10 or at P18 (not shown). Furthermore, the R_m of FS cells in wild-type (WT) mice at ≥P18 is identical in Kv3.1/Kv3.2 double knockout (DKO) mice (not shown).

Multiple factors could contribute to a developmental increase in resting membrane conductance in FS cells. Possibilities include an increase in spontaneous evoked excitatory and/or inhibitory synaptic activity, tonic GABAergic activity, increased gap-junctional coupling between FS cells (Amitai et al. 2002), changes in neuronal architecture (such as increased somatodendritic area), or an increased "leak" conductance at rest mediated by K^+, Na^+, and/or other ions. Indeed, some of these factors do contribute to the changes in FS cell input resistance (see Discussion). However, we found that

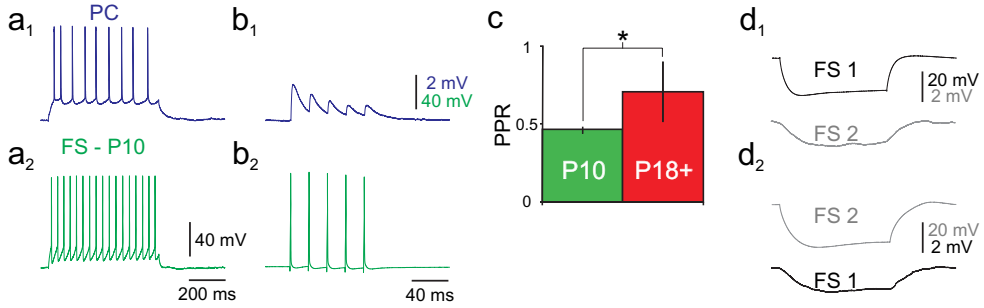

Figure 5. Chemical FS cell-to-pyramidal and electrical FS cell-to-FS cell transmission at P10 versus P18+. (*a*) Dual whole-cell recording of an FS cell→PC pair in layer 2/3 barrel cortex at P10. PC (a_1) and FS cell (a_2) firing patterns are shown. (*b*) APs generated in the presynaptic FS cell (5 at 40 Hz) generated unitary GABA-mediated postsynaptic potentials in the postsynaptic PC, recorded as depolarizing events. (*c*) Summary data illustrating greater paired-pulse depression at FS cell→PC connections at P10 relative to P18+. (*d*) Example of an electrical connection between neighboring FS cells at P10. In d_1, a hyperpolarizing current injection (−200 pA in this example) to FS cell #1 evoked a hyperpolarizing response in FS cell #2 (average of 20 sweeps); in d_2, a hyperpolarizing current injection to FS cell #2 generated a reciprocal hyperpolarization in FS cell #1.

spontaneous excitatory and inhibitory synaptic input to FS cells was high at P10 and P18+ and that blockade of neurotransmission at both ages had small (but definite) effects on R_m at rest (not shown). In addition, while a component of membrane leak derives from gap-junctional connections, we also found frequent electrical coupling of similar coupling coefficients between FS cells at P10 as at P18+ (see above). Hence, our data suggested that a prominent component of the change in FS cell membrane resistance between P10 and P18+ was due to the developmental upregulation of ionic leak conductances.

Developmental Regulation of Subthreshold-Operating K+ Currents in FS Cells

We argue here that a major determinant of the decrease in membrane resistance during postnatal development of FS cells is an increase in the ionic conductances active at rest.

FS cell RMP decreases (i.e., becomes more negative/hyperpolarized) with postnatal age in parallel with the decrease in R_m (Table 1), suggesting an increase in K^+ permeability relative to Na^+ permeability.

Several types of K^+ channels can contribute to subthreshold K^+ permeability. These include Kv1, Kv4, and Kv7 (or M-type) subthreshold-activating voltage-gated channels, inward rectifiers (K_{ir}), and 2-pore K^+ leak channels (K_{2P}). Kv1 and Kv4 channels do not contribute to the FS cell resting leak conductance since application of dendrotoxins (which block Kv1 channels) and 5 mM 4-amiopyridine (4-AP, which blocks Kv4 channels as well as Kv1 and Kv3 channels) had no effect on FS cell RMP or R_m calculated at rest (data not shown; see also Goldberg et al. 2008). We then performed detailed voltage clamp analysis at 2 time points (P10 and P18) to gain more information concerning the ionic currents that operate near rest in FS cells.

We employed a slow voltage ramp protocol to isolate steady-state currents (see Materials and Methods). Voltage was ramped from –125 to –45 mV, at a rate of 20 mV/s. The current response to this voltage ramp can be converted to a time-independent *I-V* plot. At potentials close to RMP, the slope of this *I-V* plot was much greater at P18 than at P10 (Fig. 6*a*), consistent with the developmental difference in R_m at these 2 ages. The slope of the *V-I* plot (i.e., the resistance) was 241.0 ± 73.9 at P10 (n = 3) and 108.6 ± 21.3 (n = 4) at P18 (note that voltage clamp recording conditions differed from current clamp experiments; see Materials and Methods). Of further interest, while the steady-state current–voltage relationship was near-linear at P10, there was a marked inwardly rectifying component at P18 (Fig. 6).

The inwardly rectifying appearance of the modified *I-V* plot in mature cells suggested the presence of a developmentally regulated inwardly rectifying K^+ current, likely mediated by K_{ir} channels. Such a current operates at/near RMP, where it can contribute to the passive membrane properties of FS cells. That the slope of the *I-V* plot at potentials more positive than RMP (i.e., at the reversal potential of the *I-V* plot; see Fig. 6*a*) was also steeper at P18 suggests a contribution from K_{2P} channels to the developmental difference in leak conductances between P10 and P18 FS cells. However, the pharmacologic tools available to differentiate the relative contributions of these 2 (or other) subthreshold currents at present are limited.

We first investigated which K_{ir} subunits are expressed in FS cells. For this purpose, we performed RT-PCR of RNA extracted from neocortical FS cells purified from PV-GFP transgenic mice via FACS (see Materials and Methods). Members of 3 (of 7) K_{ir} subfamilies were consistently expressed in FS neurons (K_{ir}2, 3, and 6; not shown), with prominent expression of 2 members of the K_{ir}2 subfamily (K_{ir}2.2 and 2.3), 2 members of the K_{ir}3 subfamily (K_{ir}3.1 and 3.3), and 1 member of the K_{ir}6 subfamily (K_{ir}6.2) (Fig. 7*e*). We also noted a few samples positive for K_{ir}4.1; however, we attributed this to low-level contamination by glia, as previous immunohistochemistry for K_{ir}4.1 produces glial-specific staining (Higashi et al. 2001) and K_{ir}4.1-EGFP transgenic mice (Tang et al. 2009) do not express GFP in neocortical neurons (EM Goldberg, B Rudy, unpublished data). K_{ir}3 subunits mediate the G protein–activated inward rectifier channels (GIRKs) which are known to be ubiquitously expressed in neocortex; however, these channels are believed to require activation via second messenger systems and are thus unlikely to contribute to the observed constitutively active inward rectifier current seen here (see Discussion). K_{ir}6 subunits are components of adenosine triphosphate (ATP)-sensitive K^+ channels (K_{ATP}), which may be present in FS cells (EM Goldberg, B Rudy, unpublished data; Zawar et al. 1999; Zawar and Neumcke 2000). However, these channels are activated when ATP concentrations are low and are thus also unlikely to mediate the observed inwardly rectifying current. Furthermore, glibenclamide, a blocker of K_{ATP} channels, had no

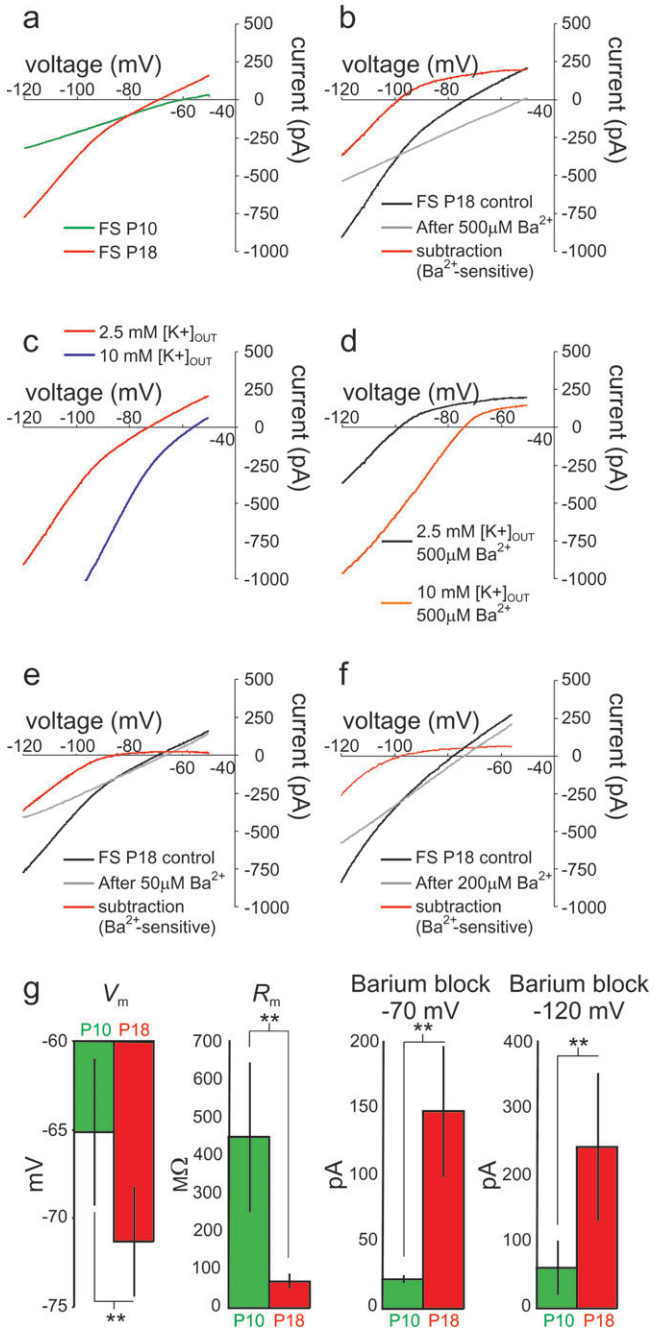

Figure 6. Developmental regulation of leak currents in FS cells. (*a*) Modified *I-V* plot (see Materials and Methods) illustrating the current recorded in a P10 ("green") and P18 ("red") FS cell in response to a 4-s voltage ramp from −125 to −45 mV (at 20 mV/s). Note that, while the *I-V* plot at P10 is nearly linear, the *I-V* plot at P18 exhibits a markedly steeper slope with a prominent inwardly rectifying component. (*b*) 500 μM Ba^{2+} blocks the inwardly rectifying component of the *I-V* curve at P18. Shown are control traces ("black"), traces after application of 500 μM Ba^{2+} ("gray"), and the Ba^{2+}-sensitive subtraction current (red; black minus gray). Note that the *I-V* plot after application of Ba^{2+} is near-linear and exhibits a slope similar to the P10 curve (compare the gray curve in Fig. 6*b* to the green curve in Fig. 6*a*). (*c*) The Ba^{2+}-sensitive current is a K^+ current. Shown in Figure 6*c* is the same cell as in Figure 6*b*, illustrating that increasing the external potassium concentration ($[K^+]_{OUT}$) from 2.5 (red) to 10 mM (blue) shifts the *I-V* plot to the right, with a commensurate shift in the rectification point. In addition, the reversal potential of the Ba^{2+}-sensitive current shifts to the right, in accordance with the change in E_K. (*d*) Shown are the currents blocked by 500 μM Ba^{2+} in 2.5 mM (black) and 10 mM (red) $[K^+]_{OUT}$. Note that the inward component of the Ba^{2+}-sensitive current is larger with increased $[K^+]_{OUT}$ and that the rectification point is shifted to the right, consistent with blockade of an inward rectifier K+ current component. (*e*) Different cell, illustrating the effect of 50 μM Ba^{2+}. (*f*) Different cell, illustrating the effect of 200 μM Ba^{2+}. (*g*) Summary data illustrating the change in V_m and R_m produced by 500 μM Ba^{2+} as well as the magnitude of the current blocked by 500 μM Ba^{2+} at −70 and −120 mV at P10 (green) and P18+ (red).

effect on RMP or R_m (not shown). These results suggest that the inwardly rectifying current in FS cells is mediated by K_{ir} channels containing $K_{ir}2$ subunits, which are the major mediators of strong inward rectifier currents in brain neurons.

We then used qPCR of FACS-purified FS cells to investigate which $K_{ir}2$ transcripts are upregulated in FS cells during postnatal development. These experiments confirmed that $K_{ir}2.2$ and $K_{ir}2.3$ are the main $K_{ir}2$ transcripts in FS cells and that the levels of both increase between P10 and P18 (Fig. 7*d*).

We also used qPCR of FS cell RNA to investigate which K_{2P} subunits are expressed in FS cells and which (if any) are upregulated during development (Fig. 7). Transcripts of 4 K2P proteins were prominently detected in FS cells, $K_{2P}1.1$ (also known as TWIK-1), $K_{2P}2.1$ (TREK-1), $K_{2P}3.1$ (TASK-1), and $K_{2P}9.1$ (TASK-3). The levels of 2 of these ($K_{2P}1.1$ and $K_{2P}9.1$) were significantly higher in P18 FS cells compared with cells isolated from P10 mice (>2-fold increase). TWIK-1 ($K_{2P}1.1$) and TASK-3 ($K_{2P}9.1$) are also the most abundant K_{2P} transcripts in FS cells at P18 (Fig. 7*d*). These results indicate that TWIK-1 and TASK channels (perhaps as TASK-1/TASK-3 heteromultimeric complexes) contribute to the large K^+ leak of FS cells at P18+. We also noted prominent $K_{2P}2.1$ expression at P10, with levels decreasing during development.

Electrophysiological and Pharmacological Characterization of Leak Currents in FS Cells

As mentioned above, the lack of pharmacological agents available for selective blockade of K_{2P} and K_{ir} channels prevented us from separating the relative contributions of these channels to the FS cell leak conductance. Instead, we tested the nonspecific K^+ channel blocker barium (Ba^{2+}). At sufficient concentrations, Ba^{2+} blocks many types of K^+ channels; however, K_{ir} channels and members of the $K_{ir}2$ subfamily in particular exhibit the greatest sensitivity to Ba^{2+} block (Kubo et al. 1993; Coetzee et al. 1999; Lopatin and Nichols 2001; Adelman et al. 2009). Several K_{2P} channels are also blocked by Ba^{2+} (Plant et al. 2009); however, blockade of K_{2P} channels in general requires higher concentrations of Ba^{2+}.

We tested the effect of Ba^{2+} at concentrations ranging from 50 to 500 μM on the currents elicited in response to voltage ramps (as above) delivered to P18+ FS cells (Fig. 6). The lowest concentrations (i.e., ⩾50 μM) should block the inward component of all $K_{ir}2$ channels. The higher concentrations tested (100–500 μM) will also partially block some K_{2P} channels, to varying degrees. We found that 50 μM Ba^{2+} completely blocked the inward component of the inward rectifying current described above (Fig. 6*e*) and had a small effect on the reversal potential; in addition, 50 μM Ba^{2+} produced an increase in R_m (measured using the slope of the outward component of the *I-V* plot) from 118.7 ± 20.1 to 130.7 ± 14.7 MΩ ($n = 5$; $P = 0.06$). Higher concentrations of Ba^{2+} produced progressively greater effects on the reversal potential and slope of the I-V curve (Fig. 6*b*,*f*) and produced a large increase in R_m (from 112.3 ± 16.3 to 153.1 ± 2.0 MΩ; $n = 4$; $P < 0.01$ for 500 μM Ba^{2+}). Five hundred micro molar Ba^{2+} also produced a dramatic shift in the reversal potential of the *I-V*

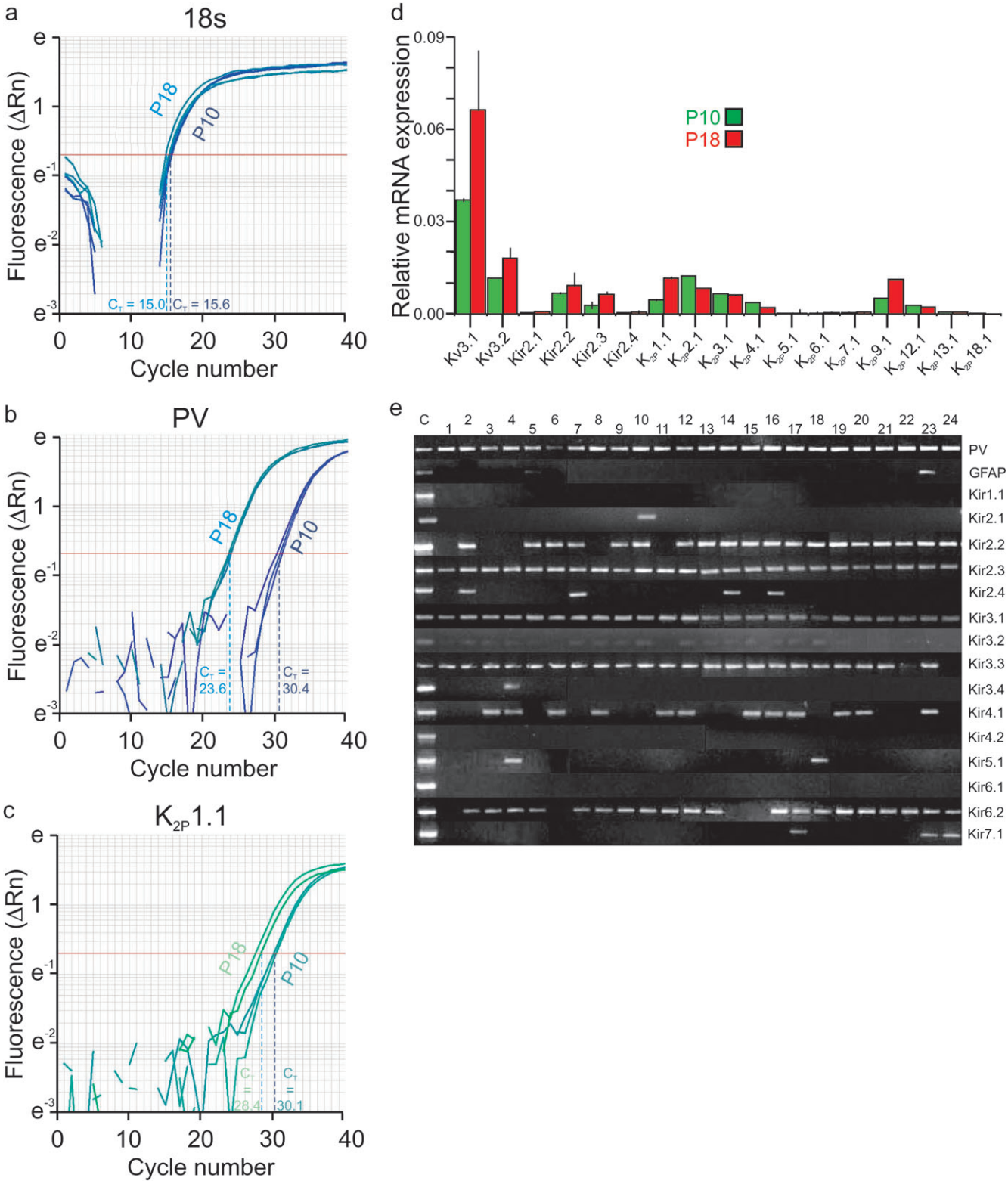

Figure 7. FS cells display a developmental upregulation of $K_{ir}2$ and K_{2P} channels. (*a*) Sample qPCR reaction for 18s RNA. On the *y*-axis is Rn, a normalized reporter signal that represents the cycle-by-cycle ratio of reporter dye and reference dye for each sample (ΔRn = Rn – baseline). Threshold cycle number (C_T) which corresponds to the PCR cycle number at which the reaction reaches a threshold level is indicated by a horizontal red line. For 18s RNA, C_T was 15.6 ± 0.02 at P10 and 15.06 ± 0.15 at P18. (*b*) qPCR amplification plot for PV, as in *a* above. For PV, C_T was 23.59 ± 0.09 at P18 and 30.44 ± 0.21 at P10. (*c*) qPCR amplification plot for $K_{2P}1.1$. C_T was 30.1 ± 0.11 at P10 and 28.4 ± 0.61 at P18. (*d*) Bar plot of qPCR results at P10 ("green") and P18 ("red"). Data are shown as expression relative to a reference transcript (18s RNA) to yield a normalized value. All qPCR reactions were performed in triplicate (i.e., $n = 3$). Data are expressed as mean ± SD. Note that $K_{2P}4.1$ and $K_{2P}12.1$ exist at very low levels and are not developmentally-regulated at P10 and P18. (*e*) RT-PCR reaction performed with 1 μL cDNA from FACS-sorted FS cells (for details, see text). Note prominent expression of PV, a marker of neocortical FS cells, in all (24 of 24) reactions, and absence of the glial marker GFAP in nearly all (23 of 24).

plot of 20.4 ± 1.0 mV, from −69.8 ± 2.8 to −49.5 ± 2.8 mV (n = 4; P < 0.01) (Fig. 6*g*). These data suggest that, in addition to K_{ir} channels sensitive to low concentrations of Ba^{2+} (i.e., 50 μM), FS cells at P18+ also express K^+ leak channels sensitive to Ba^{2+} in the 100–500 μM range.

At P18+, bath application of low concentrations of Ba^{2+} (50 μM) blocked 27.5 ± 19.9 pA of outward holding current (i.e., the current required to voltage clamp the cell at −70 mV; mean ± SD; n = 5), while 500 μM Ba^{2+} blocked 148.1 ± 49.1 pA of outward holding current (mean ± SD; n = 8; P < 0.01 vs. 50 μM) (Fig. 6*b*,*e*). However, at −120 mV, 50 μM Ba^{2+} blocked the same amount of current as 500 μM Ba^{2+} (50 μM Ba^{2+}, 343.8 ± 122.2 pA; 500 μM Ba^{2+}, 302.8 ± 138.3 pA, P > 0.05 vs. 50 μM Ba^{2+}) (Fig. 6*f*). In contrast to the effects of 500 μM Ba^{2+} on FS cells at age ≥P18, we found that, at P10, 500 μM Ba^{2+} blocked only 21.8 ± 2.8 pA of outward holding current at −70 mV (mean ± SD; n = 5; P < 0.01 compared with data at P18+; Fig. 6*g*). In addition, we found that the maximal Ba^{2+}-sensitive inward current (measured at −120 mV) was markedly less at P10 (−75.5 ± 51.3 pA) than at P18 (−302.8 ± 138.3 pA; P < 0.01) (Fig. 6*g*), consistent with the lack of inward rectification of the whole-cell current at P10.

The Ba^{2+}-sensitive current was confirmed to be a K^+ current, as it reversed near the predicted K^+ equilibrium potential (E_K) (−95.1 ± 10.1 mV; mean ± SD; n = 8; Fig. 6*d*). In addition, the inward component of the Ba^{2+}-sensitive current increased in amplitude with elevated extracellular K^+ ($[K^+]_{OUT}$) (Fig. 6*c*), an effect that was accompanied by a rightward shift in the reversal potential of the whole-cell current as well as in the rectification point of the Ba^{2+}-sensitive current in accordance with the change in E_K (Fig. 6*d*).

We also tested the effect of Ba^{2+} on FS cells in layer II/III mouse barrel cortex in current clamp mode. In the presence of 10 μM CNQX and 50 μM D-APV (blockers of AMPA- and N-methyl-D-aspartic acid type glutamate receptors, respectively), application of 50 μM Ba^{2+} (at P18+) produced a small depolarization of 3.6 ± 0.3 mV (n = 3), which was qualitatively similar to and not statistically different than the effect of this Ba^{2+} concentration on the reversal potential of the whole-cell current obtained in the voltage clamp experiments (P = 0.52 vs. voltage clamp data). Increasing concentrations of Ba^{2+} produced still larger depolarizations. Bath application of 500 μM Ba^{2+} produced a depolarization of 17.3 ± 0.4 mV (n = 12), such that FS cells began to fire spontaneously in most (10 of 12) experiments and at high frequency (Fig. 8). There was also a large increase in the frequency of high-frequency spontaneous IPSPs, which were blocked by 10 μM SR-9531 (gabazine; blocker of $GABA_A$ receptors), (Fig. 8*b*). The Ba^{2+}-induced spontaneous firing and the increase in GABA-mediated PSP frequency were blocked by 500 nM TTX; However, TTX did not block the Ba^{2+}-induced depolarization (18.4 ± 0.3 mV; n = 3; P > 0.05 vs. 500 μM Ba^{2+} alone) (Fig. 8*c*). These results suggest that the increase in IPSPs in response to 500 μM Ba^{2+} were produced by APs generated in other, synaptically connected FS cells that were also depolarized to firing by Ba^{2+}. The Ba^{2+}-induced depolarization was accompanied by an increase in apparent R_m (as monitored using continuous 100 ms, −100 pA current pulses at 0.1 Hz), from 81.2 ± 24.4 to 150.4 ± 36.4 MΩ (mean ± SD, n = 6; P < 0.01).

To confirm that the large Ba^{2+}-induced depolarization was not an artifact of having dialyzed the normal intracellular constituents of the cell via whole-cell clamp, we performed gramicidin perforated patch recordings of FS cells and found that the modified I-V curve of FS cells appeared qualitatively similar (i.e., inwardly rectifying; data not shown) and that 500 μM Ba^{2+} produced a depolarization that was identical in amplitude to that observed with whole-cell clamp (not shown). In addition, we performed cell-attached current clamp recordings and found in this noninvasive recording configuration that application of 500 μM Ba^{2+} produced spontaneous AP discharge (Supplementary Fig. S3*a*).

In conclusion, we propose that FS cells express a developmentally regulated conductance that strongly modulates FS cell intrinsic excitability via control of RMP and R_m. This conductance is a composite of a strong inward rectifier and linear leak K^+ currents. Fifty micromolar Ba^{2+} (at least partially) blocks a strong $K_{ir}2$-mediated inward rectifier that is upregulated during postnatal development and contributes to the RMP

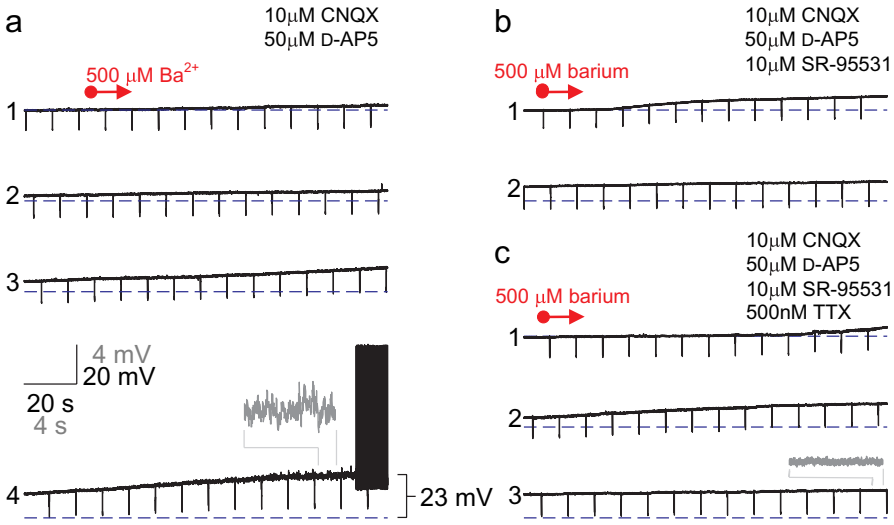

Figure 8. Ba^{2+} depolarizes FS cells, producing spontaneous high-frequency firing. (*a*) Bath application of 500 μM Ba^{2+} (indicated by "red arrow") produces depolarization of an FS cell to the point of AP firing. Successive 5-min segments of the current clamp recording are shown (indicated as 1–4). Insets ("gray") illustrate selected segments at ×5 magnification. (*b*) 500 μM Ba^{2+} produces a depolarization of similar magnitude in the presence of 10 μM SR-95531 and (*c*) 500 nM TTX.

and R_m of FS cells at/near rest. FS cells also contain a K^+ leak current likely mediated by TWIK-1 and TASK-1/3 K_{2P} channels that also contributes to the hyperpolarization and decrease in R_m of FS cells during postnatal development. Consistent with involvement of TASK channels, application of the local anesthetic bupivacaine (Supplementary Fig. S4*a*) as well as acidification of the extracellular solution (both of which are known to block TASK channels; Supplementary Fig. S4*b*) were found to increase FS cell R_m. Furthermore, the membrane resistance of FS cells was found to be approximately 2-fold larger in TASK-1/3 DKO mice (173.4 ± 112.6; $n = 8$; $P < 0.05$ vs. WT), approaching values similar to that observed in pyramidal neurons (Fig. 9*i*). The membrane time constant was also approximately 2-fold larger in TASK-1/3 DKO mice (10.9 ± 4.3; $n = 8$; $P < 0.05$ vs. WT) (Fig. 9*i*).

Subthreshold Oscillations in FS Cells: Development and Mechanism

FS cells are known to contribute to the generation and maintenance of rhythmic and oscillatory activity in cortical networks (Deans et al. 2001; Whittington and Traub 2003; Cardin et al. 2009; Sohal et al. 2009). FS cells themselves exhibit intrinsic subthreshold membrane potential oscillations in the γ-frequency range (Llinas et al. 1991; Pike et al. 2000; Goldberg et al. 2008). We confirmed that many FS cells in layer 2/3 barrel cortex exhibited high-frequency subthreshold membrane potential oscillations at P18+ (Fig. 9*d*,*e*, and *h*), with an amplitude of 2.95 ± 0.76 mV ($n = 10$; see Materials and Methods). The mean frequency of the subthreshold membrane potential oscillation among those FS cells at P18+ that did exhibit robust near-threshold oscillations (20/29 cells examined) was 52.2 ± 19.9 Hz (mean ± SD; $n = 20$). However, FS cells at P10 were noted to oscillate (5/6 cells examined) at much lower frequency (11.3 ± 1.8 Hz; mean ± SD; $n = 5$; $P < 0.05$ vs. P14–15 and <0.01 vs. P18+) (Fig. 9*a*–*c*,*h*), although the amplitude was similar (2.01 ± 0.97 mV; $n = 5$; $P > 0.05$ vs. P18+). We further found that the frequency of oscillations at P11–P17 was intermediate between that at P10 and P18+, indicating the existence of a strong, graded relationship between postnatal age and the frequency of this FS cell subthreshold membrane potential oscillation (Fig. 9*h*). We infer that the ability of FS cells to generate high-frequency subthreshold membrane potential oscillations may indeed require the low R_m and fast τ_m typical of mature FS cells. Consistent with this hypothesis, we found that the mean frequency of the FS cell subthreshold oscillation was markedly reduced in TASK-1/3 DKO mice to 32.9 ± 10.8 Hz ($n = 7$; $P < 0.05$ vs. WT mice) (Fig. 9*f*–*h*), which further supports a role for TASK-1/3 channels in FS cell oscillatory behavior. The ability of FS cells to support high-frequency subthreshold membrane potential oscillations in turn may be important for the role of these cells in the production of high-frequency activity at the level of cortical networks (Cardin et al. 2009; Haider and McCormick 2009).

Discussion

In this study, we performed electrophysiological recordings from a large sample of FS cells in primary somatosensory neocortex from mice of various ages ranging from P10 to P60. While confirming that multiple aspects of mature neocortical FS cell physiology are coordinated for rapid response, our data indicate that these features develop dramatically and coalesce during the second and third postnatal weeks. We show that the high-frequency discharge pattern and thin spikes that define the FS cell phenotype appear during this time period, driven by the developmentally regulated expression of the FS determinants, the K^+ channel subunits Kv3.1 and Kv3.2. This is paralleled by a decrease in FS cell R_m, which represents another FS cell specialization for fast signaling: a low R_m implies a fast τ_m ($=R_m \times C_m$). This will in turn limit the duration of incoming excitatory post-synaptic potentials and the window for temporal integration at the FS cell soma, promoting synchrony detection and rapid transformation of incoming excitatory synaptic input into time-locked feed-forward output. The low R_m also implies fast conduction velocity, v ($v = \lambda/\tau_m$), such that synaptic potentials are conducted from dendrites to the soma rapidly.

Using a combination of pharmacology and molecular biological techniques, we provide data suggesting that the molecular basis of this decrease in FS cell input resistance is in part the developmental upregulation of the 2-pore (K_{2P}) K^+ channel subunits TASK-1 and -3 (and perhaps TWIK-1) as well as inward rectifier (K_{ir}) K^+ channel subunits of the $K_{ir}2$ subfamily. Finally, we show data indicating that FS cells exhibit subthreshold membrane potential oscillations whose frequency is developmentally regulated during the very same time window and which are modulated by TASK-1/3 channels.

Contributions to FS Cell Membrane Resistance at Rest

Input resistance is an essential determinant of intrinsic neuronal excitability, yet the specific determinants of R_m for most neurons are poorly understood. However, a number of factors likely contribute to the developmental decrease in FS cell R_m.

An important anatomical consideration is the presence of gap-junctional coupling, which is known to exist extensively between neocortical interneurons in general and between FS cell in particular (Galarreta and Hestrin 1999; Gibson et al. 1999; Fukuda et al. 2006). Amitai et al. (2002) estimated that approximately half of the resting membrane conductance of mature FS cells is due to leak via gap junctions. However, other studies suggest a much lower contribution of gap junctions. FS cells from layer IV barrel cortex of connexin 36 knockout (Cx36-KO) mice have an R_m of 66.0 MΩ (Deans et al. 2001) compared with 50 MΩ for control, suggesting a ~25% reduction in resting leak conductance in Cx36-KO animals. Consistent with this, mefloquine (at 25 μM), which blocks Cx36 channels as well as electrical connectivity between FS cells, increases FS cell R_m from 50 to 60 MΩ in FS cells of layer IV rat barrel cortex (Cruikshank et al. 2004), suggesting a ~15% reduction in resting leak conductance after gap-junctional blockade. So while the actual contribution of gap junctions to the resting leakage conductance of FS cells and to the developmental difference in FS cell R_m between P10 and P18 remains to be established, we note that FS cells at P10 are electrically interconnected and have a similar coupling coefficient to that observed at P18 (Fig. 5*c*,*d*).

A conspicuous feature of FS cells in the acute brain slice preparation is a high frequency of spontaneous synaptic activity (EM Goldberg, B Rudy, unpublished data), which could decrease R_m at rest via a shunting mechanism. Cruikshank et al. (2004) found that blockade of glutamatergic neurotransmission

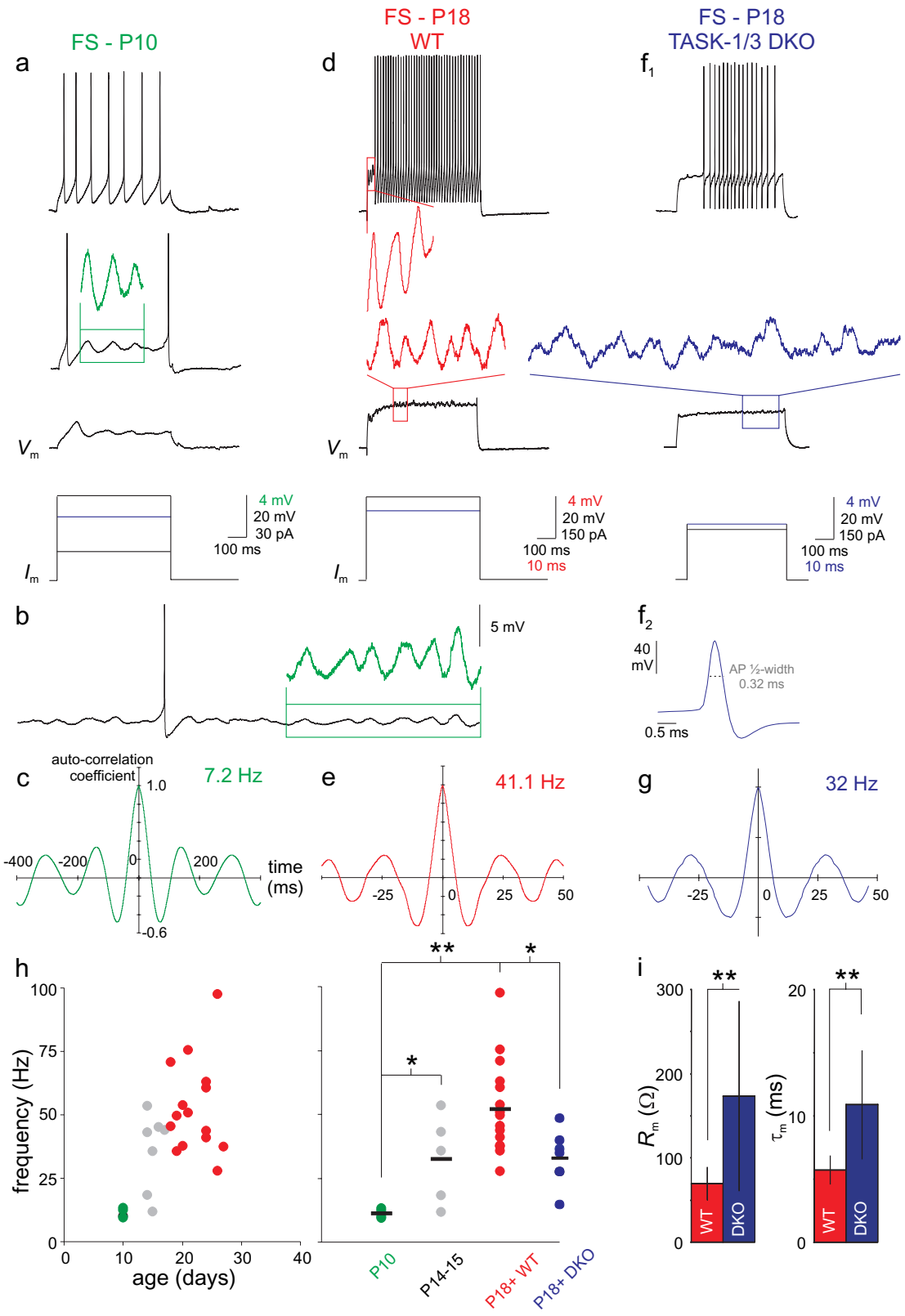

Figure 9. FS cells exhibit a developmentally regulated subthreshold membrane potential oscillation that is modulated by TASK channels. (*a*) FS cells at P10 exhibit subthreshold membrane potential oscillations at low frequency. In this example, a portion of the oscillation ("green box") is expanded 5-times in amplitude ("green"; same timescale) for clarity. (*b*) Same cell as in Figure 9*a*. Depolarization with a DC current injection generated a sustained low-frequency membrane potential oscillation. Inset shows a portion of the oscillation (green) expanded 5-times in amplitude. (*c*) Autocorrelogram of the P10 FS cell membrane potential in Figure 9*a* indicating oscillation at approximately 7 Hz. *y*-axis in *c*, *e*, and *g* indicates autocorrelation coefficient. (*d*) Firing pattern for a P18 FS cell ("top"), with high-frequency subthreshold membrane potential oscillation ("red box") shown during the characteristic FS cell delay (Goldberg et al. 2008) is expanded to the left of the trace ("red"; 5-times magnification). At "bottom" is the oscillation produced in response to a near-threshold current injection. (*e*) As in Figure 9*c*, for the P18+ FS cell in 9*d*. Oscillation occurs at approximately 41 Hz. (*f*) Discharge pattern (top) and subthreshold

produced an increase in FS cell R_m of 19.2 MΩ, (from 50 to 69.2 MΩ), suggesting that ongoing synaptic activity also makes some contribution to the conductance load at rest. Blockade of excitatory or inhibitory synaptic transmission with CNQX and D-APV had a minimal effect on FS cell R_m, while blockade of tonic GABA with gabazine or picrotoxin (in the presence of blockers of excitatory synaptic transmission) had only a small effect on FS cell membrane resistance (~10% increase; EM Goldberg, R Tremblay, B Rudy, unpublished data).

These considerations led to the conclusion that a major determinant of the low R_m of FS cells is the developmentally regulated expression of leak conductances. The progressive hyperpolarization of FS cells observed during the same developmental period (Table 1) further suggests an important contribution from subthreshold-operating K^+ channels.

In terms of ion channels, any conductance active near the RMP can contribute to the apparent R_m of a cell. Among ion channels, K^+ channels are particularly important, due to the well-known role of K^+ channels in setting the membrane potential and membrane resistance, among other basic cellular neurophysiological roles (Hille 2001).

However, while there are indeed many K^+ channels, not all K^+ channels are "subthreshold-operating" K^+ channels; that is, not all K^+ channels are open in the relevant range of voltages to contribute to subthreshold membrane properties such as the membrane resistance at rest. Subthreshold-operating K^+ channels include voltage-gated ion channels of the Kv1 and Kv4 subfamilies of voltage-gated K^+ channels and members of the KCNQ and ether a go-go families of voltage-gated K^+ channels. Such channels have voltage dependencies compatible with potential contribution to subthreshold membrane properties. Inward rectifier K^+ (K_{ir}) channels and 2-pore domain-containing K^+ (K_{2P}; or leak) channels also contribute K^+ conductance at subthreshold membrane potentials.

The interest in this field has increased with the discovery of a molecular correlate of K^+ leak (K_{2P}) K^+ channels, and subsequent work indicating a role for K_{2P} channels in regulating the subthreshold properties of central neurons (Talley et al. 2000; Meuth et al. 2003; Taverna et al. 2005). Further interest in these channels derives from the fact that they are targets of endogenous neuromodulatory substances, pH, and inhalational anesthetics.

Our electrophysiological, pharmacologic, and molecular biological data indicate that a major determinant of the low R_m of FS cells is the developmentally regulated expression of a K^+ leak conductances composed of K_{2P} and K_{ir} channels.

K_{2P} channels are insensitive to classical K^+ channel blockers such as 4-AP, TEA, and cesium (Lesage 2003); however, half of the 15 known K_{2P} channels have been reported to be to some extent Ba^{2+} sensitive (Goldstein et al. 2005). Hence, we used Ba^{2+} in our initial analysis, arguing that the effects of 500 μM Ba^{2+} is due to at least partial block of a linear leak mediated by K_{2P} channels in addition to blockade of a strong inward rectifier ($K_{ir}2$).

THIK-1 is 60% blocked by 1 mM Ba^{2+} at +60 mV in heterologous expression systems (Rajan et al. 2001), but there is little or no apparent block at hyperpolarized potentials. Furthermore, THIK-1 is not expressed in neocortex, and heterologously expressed current displays moderate "outward" rectification in 2 mM $[K^+]_{OUT}$ (Rajan et al. 2001). Hence, THIK-1 is unlikely to be a component of the Ba^{2+}-sensitive current in FS cells.

TREK-1 is putatively Ba^{2+}-sensitive and expressed in neocortex as determined by in situ hybridization (Talley et al. 2001) as well as northern blot and real-time RT-PCR (Meadows et al. 2000). However, TREK-1 is also outwardly rectifying in physiological $[K^+]_{OUT}$ and is only ~20% blocked by 100 μM Ba^{2+} (Meadows et al. 2000). Our qPCR data indicated that FS cells express TREK-1, although expression of this transcript was found to decrease during development.

TALK-1 and TALK-2/TASK-4 are outwardly rectifying in physiological K^+ (Decher et al. 2001; Girard et al. 2001). In addition, expression of these channels is pancreas specific (i.e., not expressed in brain; Girard et al. 2001). While heterologously expressed TALK-2/TASK-4 does display sensitivity to Ba^{2+} (albeit at 2 mM and at alkaline pH), these channels are essentially blocked at physiological pH (Decher et al. 2001). Hence, we did not consider these channels as candidates for the K_{2P}-mediated leak in FS cells.

TWIK-1 appears to be prominently expressed in FS cells in a developmentally regulated fashion (see Fig. 7*d*), is known to be expressed in brain (Lesage et al. 1996), and is to some extent Ba^{2+} sensitive. However, TWIK-1 is known to be inactive in the plasma membrane due to covalent modification via sumoylation (via small ubiquitin-related modifier protein 1 or SUMO-1), while desumoylation by SUMO-specific protease (SENP) reveals channel activity (Rajan et al. 2005). This is a complicated and controversial issue that is not yet resolved (Feliciangeli et al. 2007). Given the lack of specific pharmacological agents, we were unable to assess the contribution of TWIK-1 to the developmentally regulated K^+ leak current of FS cells.

Thus, we consider TASK channels, likely in the form of TASK-1/3 heteromultimers, to represent a significant contribution to the FS cell K^+ leak current. Similar to the current recorded here, TASK-1 has been previously shown to be insensitive to relevant concentrations of 4-AP, dendrotoxin, margatoxin, and charybdotoxin but to be partially sensitive to 100 μM Ba^{2+} and very sensitive to the anesthetic bupivacaine (Leonoudakis et al. 1998) as well as being blocked by external pH (pH = 6.7; Rajan et al. 2000). Okaty et al. (2009) recently observed a developmental increase in TASK-1 expression in FS cells using microarrays. We show here via qPCR on FACS-purified cells that FS cells express TASK-1 and -3; levels of TASK-3 were increased at P18 as compared with P10. As TASK-1 is known to form heterodimers with TASK-3 in heterologous expression systems and electrophysiological studies support the existence of TASK-1/3 heterodimerization (Goldstein et al. 2005), we hypothesize that the FS cell K^+ leak current includes TASK-1/3 heteromers, consistent with our results from TASK-1/3 DKO mice.

membrane potential oscillation (bottom) in a P18 FS cell from the TASK-1/3 DKO mouse. FS cells from these mice retained the high-frequency firing typical of FS cells. "Inset" illustrates a brief single spike (0.32 ms) at higher magnification from the same FS cell at top. (*g*) Autocorrelogram corresponding to *f*. (*h*) The frequency of the FS cell subthreshold membrane potential oscillation is age dependent and reduced in TASK-1/3 DKO mice. "At left," a plot of oscillation frequency versus age (green; P10; "gray," P11–P17; red, P18+). "At right," the frequency of the subthreshold membrane potential oscillation across cells at P10, P14–P15, P18+ WT and P18+ TASK-1/3 DKO mice are binned to clearly illustrate the range in values and cell-to-cell variability, with the mean value indicated by a horizontal "black" hatch mark. (*i*) Summary data comparing R_m (left) and τ_m (right) for FS cells from WT (red) and TASK-1/3 DKO ("blue") mice (see text). Asterisks indicate $P < 0.05$ and double asterisks indicate $P < 0.01$ for 9*h* and *i*.

The powerful effects of Ba^{2+} described here suggest that modulation of the FS cell K^+ leak conductance by endogenous neuromodulators would have dramatic effects on the excitability of FS cells. FS cells are known to be modulated by various neurotransmitters (reviewed in Bacci et al. 2005). For example, serotonin (Xiang and Prince 2003), dopamine (via D_1/D_5 receptors; Gorelova et al. 2002), and noradrenergic activation (Kawaguchi and Shindou 1998) have been previously shown to produce depolarization of FS cells. The action of these endogenous substances on FS cells may be via blockade of the same channels targeted by Ba^{2+} in our experiments, and the dramatic effects of Ba^{2+} indicates the potential for a powerful modulatory influence. Our results further imply that the modulation of TASK channels in FS cells may contribute to the effects of anesthetics and acidosis on global brain function.

FS Cell Subthreshold Membrane Potential Oscillations: Developmental Regulation and Modulation by TASK Channels

We showed that the high-frequency subthreshold membrane potential oscillations that typify FS cells (Llinas et al. 1991; Pike et al. 2000) also develop during the second and third postnatal weeks, in parallel with emergence of fast spiking FS and low input resistance. This may have important consequences for the known function of FS cells in generating γ-band activity in neocortex (Cardin et al. 2009). Interestingly, the time course of the changes in FS cells reported here at the cellular level also parallel the developmental emergence of "ripple" oscillations in hippocampus (Buhl and Buzsaki 2005). The slow response properties, slow membrane time constant, and low-frequency subthreshold oscillations of young FS cells may partially explain why these cells are not efficiently driven by thalamic input in the developing neocortex (Daw et al. 2007) but act as powerful sources of feed-forward inhibition in mature thalamocortical circuits. Our results may also explain the recent finding of impaired network oscillations in TASK-3 knockout mice (Pang et al. 2009).

Funding

National Institutes of Health (grants NS30989 and NS045217 to B.R.); National Research Service Award (F30 NS47882 to E.M.G).

Supplementary Material

Supplementary material can be found at: http://www.cercor.oxfordjournals.org/

Notes

We thank Z. Josh Huang for the gift of PV-GFP transgenic mice, Douglas A. Bayliss for the gift of TASK 1/3 DKO mice, Madison D. Harrell and William A. Coetzee for assistance with qPCR methodology and the gift of PCR primers, Corinna Klein for assistance with the use of FACS, and Max Schiff for valuable discussions. *Conflict of Interest*: None declared.

References

Adelman JP, Clapham DE, Hibino H, Inanobe A, Jan LY, Karschin A, Kubo Y, Kurachi Y, Lazdunski M, Miki T, et al. Inwardly rectifying potassium channels [Internet]. Last modified on 2009-10-14. IUPHAR database (IUPHAR-DB). [cited 2010 July 29]. Available from: URL http://www.iuphar-db.org/DATABASE/FamilyMenuForward?familyId=74.

Amitai Y, Gibson JR, Beierlein M, Patrick SL, Ho AM, Connors BW, Golomb D. 2002. The spatial dimensions of electrically coupled networks of interneurons in the neocortex. J Neurosci. 22:4142–4152.

Angulo MC, Lambolez B, Audinat E, Hestrin S, Rossier J. 1997. Subunit composition, kinetic, and permeation properties of AMPA receptors in single neocortical nonpyramidal cells. J Neurosci. 17:6685–6696.

Angulo MC, Staiger JF, Rossier J, Audinat E. 2003. Distinct local circuits between neocortical pyramidal cells and fast-spiking interneurons in young adult rats. J Neurophysiol. 89:943–953.

Atzori M, Lau D, Tansey EP, Chow A, Ozaita A, Rudy B, McBain CJ. 2000. H2 histamine receptor-phosphorylation of Kv3.2 modulates interneuron fast spiking. Nat Neurosci. 3:791–798.

Bacci A, Huguenard JR, Prince DA. 2005. Modulation of neocortical interneurons: extrinsic influences and exercises in self-control. Trends Neurosci. 28:602–610.

Bartos M, Vida I, Jonas P. 2007. Synaptic mechanisms of synchronized gamma oscillations in inhibitory interneuron networks. Nat Rev Neurosci. 8:45–56.

Beierlein M, Gibson JR, Connors BW. 2003. Two dynamically distinct inhibitory networks in layer 4 of the neocortex. J Neurophysiol. 90:2987–3000.

Ben-Ari Y. 2002. Excitatory actions of GABA during development: the nature of the nurture. Nat Rev Neurosci. 3:728–739.

Buhl DL, Buzsaki G. 2005. Developmental emergence of hippocampal fast-field "ripple" oscillations in the behaving rat pups. Neuroscience. 134:1423–1430.

Cardin JA, Carlén M, Meletis K, Knoblich U, Zhang F, Deisseroth K, Tsai LH, Moore CI. 2009. Driving fast-spiking cells induces gamma rhythm and controls sensory responses. Nature. 459:663–667.

Chattopadhyaya B, Di Cristo G, Higashiyama H, Knott GW, Kuhlman SJ, Welker E, Huang ZJ. 2004. Experience and activity-dependent maturation of perisomatic GABAergic innervation in primary visual cortex during a postnatal critical period. J Neurosci. 24:9598–9611.

Chow A, Erisir A, Farb C, Nadal MS, Ozaita A, Lau D, Welker E, Rudy B. 1999. K(+) channel expression distinguishes subpopulations of parvalbumin- and somatostatin-containing neocortical interneurons. J Neurosci. 19:9332–9345.

Coetzee WA, Amarillo Y, Chiu J, Chow A, Lau D, McCormack T, Moreno H, Nadal MS, Ozaita A, Pountney D, et al. 1999. Molecular diversity of K+ channels. Ann N Y Acad Sci. 868:233–285.

Connors BW, Gutnick MJ. 1990. Intrinsic firing patterns of diverse neocortical neurons. Trends Neurosci. 13:99–104.

Cruikshank SJ, Hopperstad M, Younger M, Connors BW, Spray DC, Srinivas M. 2004. Potent block of Cx36 and Cx50 gap junction channels by mefloquine. Proc Natl Acad Sci U S A. 101:12364–12369.

Cruikshank SJ, Lewis TJ, Connors BW. 2007. Synaptic basis for intense thalamocortical activation of feedforward inhibitory cells in neocortex. Nat Neurosci. 10:462–468.

Daw MI, Ashby MC, Isaac JT. 2007. Coordinated developmental recruitment of latent fast spiking interneurons in layer IV barrel cortex. Nat Neurosci. 10:453–461.

Deans MR, Gibson JR, Sellitto C, Connors BW, Paul DL. 2001. Synchronous activity of inhibitory networks in neocortex requires electrical synapses containing connexin36. Neuron. 31:477–485.

Decher N, Maier M, Dittrich W, Gassenhuber J, Bruggemann A, Busch AE, Steinmeyer K. 2001. Characterization of TASK-4, a novel member of the pH sensitive, two-pore domain potassium channel family. FEBS Lett. 492:84–89.

Doischer D, Hosp JA, Yanagawa Y, Obata K, Jonas P, Vida I, Bartos M. 2008. Postnatal differentiation of basket cells from slow to fast signaling devices. J Neurosci. 28:12956–12968.

Du J, Zhang L, Weiser M, Rudy B, McBain CJ. 1996. Developmental expression and functional characterization of the potassium-channel subunit Kv3.1b in parvalbumin-containing interneurons of the rat hippocampus. J Neurosci. 16:506–518.

Feliciangeli S, Bendahhou S, Sandoz G, Gounon P, Reichold M, Warth R, Lazdunski M, Barhanin J, Lesage F. 2007. Does sumoylation control K2P1/TWIK1 background K+ channels? Cell. 130:563–569.

Fukuda T, Kosaka T, Singer W, Galuske RA. 2006. Gap junctions among dendrites of cortical GABAergic neurons establish a dense and widespread intercolumnar network. J Neurosci. 26:3434–3443.
Gabernet L, Jadhav SP, Feldman DE, Carandini M, Scanziani M. 2005. Somatosensory integration controlled by dynamic thalamocortical feed-forward inhibition. Neuron. 48:315–327.
Galarreta M, Hestrin S. 1998. Frequency-dependent synaptic depression and the balance of excitation and inhibition in the neocortex. Nat Neurosci. 1:587–594.
Galarreta M, Hestrin S. 1999. A network of fast-spiking cells in the neocortex connected by electrical synapses. Nature. 402:72–75.
Gandhi SP, Yanagawa Y, Stryker MP. 2008. Delayed plasticity of inhibitory neurons in developing visual cortex. Proc Natl Acad Sci U S A. 105:16797–16802.
Geiger JR, Lübke J, Roth A, Frotscher M, Jonas P. 1997. Submillisecond AMPA receptor-mediated signaling at a principal neuron-interneuron synapse. Neuron. 18:1009–1023.
Geiger JR, Melcher T, Koh DS, Sakmann B, Seeburg PH, Jonas P, Monyer H. 1995. Relative abundance of subunit mRNAs determines gating and Ca2+ permeability of AMPA receptors in principal neurons and interneurons in rat CNS. Neuron. 15:193–204.
Gibson JR, Beierlein M, Connors BW. 1999. Two networks of electrically coupled inhibitory neurons in neocortex. Nature. 402:75–79.
Girard C, Duprat F, Terrenoire C, Tinel N, Fosset M, Romey G, Lazdunski M, Lesage F. 2001. Genomic and functional characteristics of novel human pancreatic 2P domain K(+) channels. Biochem Biophys Res Commun. 282:249–256.
Goldberg EM, Clark BD, Zagha E, Nahmani M, Erisir A, Rudy B. 2008. K+ channels at the axon initial segment dampen near-threshold excitability of neocortical fast-spiking GABAergic interneurons. Neuron. 58:387–400.
Goldberg EM, Rudy B. 2005. Molecular contributions to the subthreshold properties of FS cells in mouse medial prefrontal cortex. SFN Abstracts. 736.2.
Goldberg EM, Watanabe S, Chang SY, Joho RH, Huang ZJ, Leonard CS, Rudy B. 2005. Specific functions of synaptically localized potassium channels in synaptic transmission at the neocortical GABAergic fast-spiking cell synapse. J Neurosci. 25:5230–5235.
Goldberg JE, Lacefield CO, Yuste R. 2004. Global dendritic calcium spikes in mouse layer 5 low threshold spiking interneurons: implications for control of pyramidal cell bursting. J Physiol. 558:465–478.
Goldstein SA, Bayliss DA, Kim D, Lesage F, Plant LD, Rajan S. 2005. International Union of Pharmacology. LV. Nomenclature and molecular relationships of two-P potassium channels. Pharmacol Rev. 57:527–540.
Gorelova N, Seamans JK, Yang CR. 2002. Mechanisms of dopamine activation of fast-spiking interneurons that exert inhibition in rat prefrontal cortex. J Neurophysiol. 88:3150–3166.
Haider B, McCormick DA. 2009. Rapid neocortical dynamics: cellular and network mechanisms. Neuron. 62:171–189.
Hamam BN, Kennedy TE. 2003. Visualization of the dendritic arbor of neurons in intact 500 microm thick brain slices. J Neurosci Methods. 123:61–67.
Hefft S, Jonas P. 2005. Asynchronous GABA release generates long-lasting inhibition at a hippocampal interneuron-principal neuron synapse. Nat Neurosci. 8:1319–1328.
Hensch TK. 2005. Critical period plasticity in local cortical circuits. Nat Rev Neurosci. 6:877–888.
Higashi K, Fujita A, Inanobe A, Tanemoto M, Doi K, Kubo T, Kurachi Y. 2001. An inwardly rectifying K(+) channel, Kir4.1, expressed in astrocytes surrounds synapses and blood vessels in brain. Am J Physiol Cell Physiol. 281:C922–C931.
Hille B. 2001. Ion channels of excitable membranes. 3rd ed. Sunderland (MA): Sinauer.
Huang ZJ, Di Cristo G, Ango F. 2007. Development of GABA innervation in the cerebral and cerebellar cortices. Nat Rev Neurosci. 8:673.
Hull C, Isaacson JS, Scanziani M. 2009. Postsynaptic mechanisms govern the differential excitation of cortical neurons by thalamic inputs. J Neurosci. 29:9127–9136.
Itami C, Kimura F, Nakamura S. 2007. Brain-derived neurotrophic factor regulates the maturation of layer 4 fast-spiking cells after the second postnatal week in the developing barrel cortex. J Neurosci. 27:2241–2252.
Jiang B, Huang ZJ, Morales B, Kirkwood A. 2005. Maturation of GABAergic transmission and timing of plasticity in the visual cortex. Brain Res Rev. 50:126–133.
Jonas P, Bischofberger J, Fricker D, Miles R. 2004. Interneuron diversity series: fast in, fast out—temporal and spatial signal processing in hippocampal interneurons. Trends Neurosci. 27:30–40.
Kawaguchi Y. 1995. Physiological subgroups of nonpyramidal cells with specific morphological characteristics in layer II/III of rat frontal cortex. J Neurosci. 15:2638–2655.
Kawaguchi Y, Kondo S. 2002. Parvalbumin, somatostatin and cholecystokinin as chemical markers for specific GABAergic interneuron types in the rat frontal cortex. J Neurocytol. 31:277–287.
Kawaguchi Y, Kubota Y. 1996. Physiological and morphological identification of somatostatin- or vasoactive intestinal polypeptide-containing cells among GABAergic cell subtypes in rat frontal cortex. J Neurosci. 16:2701–2715.
Kawaguchi Y, Shindou T. 1998. Noradrenergic excitation and inhibition of GABAergic cell types in rat frontal cortex. J Neurosci. 18:6963–6976.
Kubo Y, Baldwin TJ, Jan YN, Jan LY. 1993. Primary structure and functional expression of a mouse inward rectifier potassium channel. Nature. 362:127–133.
Lawrence JJ, McBain CJ. 2003. Interneuron diversity series: containing the detonation—feedforward inhibition in the CA3 hippocampus. Trends Neurosci. 26:631–640.
Leonoudakis D, Gray AT, Winegar BD, Kindler CH, Harada M, Taylor DM, Chavez RA, Forsayeth JR, Yost CS. 1998. An open rectifier potassium channel with two pore domains in tandem cloned from rat cerebellum. J Neurosci. 18:868–877.
Lesage F. 2003. Pharmacology of neuronal background potassium channels. Neuropharmacology. 44:1–7.
Lesage F, Guillemare E, Fink M, Duprat F, Lazdunski M, Romey G, Barhanin J. 1996. TWIK-1, a ubiquitous human weakly inward rectifying K+ channel with a novel structure. EMBO J. 15:1004–1011.
Levitt P, Eagleson KL, Powell EM. 2004. Regulation of neocortical interneuron development and the implications for neurodevelopmental disorders. Trends Neurosci. 27:400–406.
Lewis DA, Hashimoto T, Volk DW. 2005. Cortical inhibitory neurons and schizophrenia. Nat Rev Neurosci. 6:312–324.
Llinas RR, Grace AA, Yarom Y. 1991. In vitro neurons in mammalian cortical layer 4 exhibit intrinsic oscillatory activity in the 10- to 50-Hz frequency range. Proc Natl Acad Sci U S A. 88:897–901.
Lopatin AN, Nichols CG. 2001. Inward rectifiers in the heart: an update on I(K1). J Mol Cell Cardiol. 33:625–638.
Ma Y, Hu H, Berrebi AS, Mathers PH, Agmon A. 2006. Distinct subtypes of somatostatin-containing neocortical interneurons revealed in transgenic mice. J Neurosci. 26:5069–5082.
Martina M, Jonas P. 1997. Functional differences in Na+ channel gating between fast-spiking interneurones and principal neurones of rat hippocampus. J Physiol. 505:593–603.
Meadows HJ, Benham CD, Cairns W, Gloger I, Jennings C, Medhurst AD, Murdock P, Chapman CG. 2000. Cloning, localisation and functional expression of the human orthologue of the TREK-1 potassium channel. Pflugers Arch. 439:714–722.
Meuth SG, Budde T, Kanyshkova T, Broicher T, Munsch T, Pape HC. 2003. Contribution of TWIK-related acid-sensitive K+ channel 1 (TASK1) and TASK3 channels to the control of activity modes in thalamocortical neurons. J Neurosci. 23:6460–6469.
Okaty BW, Miller MN, Sugino K, Hempel CM, Nelson SB. 2009. Transcriptional and electrophysiological maturation of neocortical fast-spiking GABAergic interneurons. J Neurosci. 29:7040–7052.
Owens DF, Kriegstein AR. 2002. Is there more to GABA than synaptic inhibition? Nat Rev Neurosci. 3:715–727.
Pang DS, Robledo CJ, Carr DR, Gent TC, Vyssotski AL, Caley A, Zecharia AY, Wisden W, Brickley SG, Franks NP. 2009. An unexpected role for TASK-3 potassium channels in network oscillations with implications for sleep mechanisms and anesthetic action. Proc Natl Acad Sci U S A. 106:17546–17551.
Pike FG, Goddard RS, Suckling JM, Ganter P, Kasthuri N, Paulsen O. 2000. Distinct frequency preferences of different types of rat

hippocampal neurones in response to oscillatory input currents. J Physiol. 15:529.
Plant LD, Bayliss DA, Kim D, Lesage F, Goldstein SAN. 2009. Two-P potassium channels. Last modified on. 2009-11-18. IUPHAR database (IUPHAR-DB). [cited 2010 July 29]. Available from: URL http://www.iuphar-db.org/DATABASE/FamilyMenuForward?familyId=79.
Pouille F, Scanziani M. 2001. Enforcement of temporal fidelity in pyramidal cells by somatic feed-forward inhibition. Science. 293:1159–1163.
Rajan S, Plant LD, Rabin ML, Butler MH, Goldstein SA. 2005. Sumoylation silences the plasma membrane leak K+ channel K2P1. Cell. 121: 37–47.
Rajan S, Wischmeyer E, Karschin C, Preisig-Müller R, Grzeschik KH, Daut J, Karschin A, Derst C. 2001. THIK-1 and THIK-2, a novel subfamily of tandem pore domain K+ channels. J Biol Chem. 276:7302–7311.
Rajan S, Wischmeyer E, Xin Liu G, Preisig-Muller R, Daut J, Karschin A, Derst C. 2000. TASK-3, a novel tandem pore domain acid-sensitive K+ channel—an extracellular histidine as pH sensor. J Biol Chem. 275:16650–16657.
Rudy B, Maffie J, Amarillo Y, Clark B, Goldbrg EM, Jeong HY, Kruglikov I, Kwon E, Nadal M, Zagha E. 2009. Structure and function of voltage-gated K+ channels: Kv1 to Kv9 subfamilies. In: Squire LR, editor. Encyclopedia of neuroscience, volume 10. Oxford: Academic Press. p. 397–425.
Rudy B, McBain CJ. 2001. Kv3 channels: voltage-gated K+ channels designed for high-frequency repetitive firing. Trends Neurosci. 24:517–526.
Sohal VS, Zhang F, Yizhar O, Deisseroth K. 2009. Parvalbumin neurons and gamma rhythms enhance cortical circuit performance. Nature. 459:698–702.
Staff NP, Jung HY, Thiagarajan T, Yao M, Spruston N. 2000. Resting and active properties of pyramidal neurons in subiculum and CA1 of rat hippocampus. J Neurophysiol. 84:2398–2408.
Stuart GJ, Sakmann B. 1995. Patch-pipette recordings from the soma, dendrites, and axon of neurons in brain slices. In: Sakmann B, Neher E, editors. Single-channel recording. 2nd ed. New York: Plenum Press. p. 199–211.
Talley EM, Lei Q, Sirois JE, Bayliss DA. 2000. TASK-1, a two-pore domain K+ channel, is modulated by multiple neurotransmitters in motoneurons. Neuron. 25:399–410.
Talley EM, Solorzano G, Lei Q, Kim D, Bayliss DA. 2001. CNS distribution of members of the two-pore-domain (KCNK) potassium channel family. J Neurosci. 21:7491–7505.
Tang X, Taniguchi K, Kofuji P. 2009. Heterogeneity of Kir4.1 channel expression in glia revealed by mouse transgenesis. Glia. 57:1706–1715.
Tansey EP, Chow A, Rudy B, McBain CJ. 2002. Developmental expression of potassium-channel subunit Kv3.2 within subpopulations of mouse hippocampal inhibitory interneurons. Hippocampus. 12:137–148.
Taverna S, Tkatch T, Metz AE, Martina M. 2005. Differential expression of TASK channels between horizontal interneurons and pyramidal cells of rat hippocampus. J Neurosci. 25:9162–9170.
Traub RD, Bibbig A, LeBeau FE, Buhl EH, Whittington MA. 2004. Cellular mechanisms of neuronal population oscillations in the hippocampus in vitro. Annu Rev Neurosci. 27:247–278.
Walsh CA, Morrow EM, Rubenstein JL. 2008. Autism and brain development. Cell. 135:396–400.
Weiser M, Bueno E, Sekirnjak C, Martone ME, Baker H, Hillman D, Chen S, Thornhill W, Ellisman M, Rudy B. 1995. The potassium channel subunit KV3.1b is localized to somatic and axonal membranes of specific populations of CNS neurons. J Neurosci. 15:4298–4314.
Whittington MA, Traub RD. 2003. Interneuron diversity series: inhibitory interneurons and network oscillations in vitro. Trends Neurosci. 26:676–682.
Xiang Z, Prince DA. 2003. Heterogeneous actions of serotonin on interneurons in rat visual cortex. J Neurophysiol. 89:1278–1287.
Zawar C, Neumcke B. 2000. Differential activation of ATP-sensitive potassium channels during energy depletion in CA1 pyramidal cells and interneurones of rat hippocampus. Pflugers Arch. 439:256–262.
Zawar C, Plant TD, Schirra C, Konnerth A, Neumcke B. 1999. Cell-type specific expression of ATP-sensitive potassium channels in the rat hippocampus. J Physiol. 514:327–341.